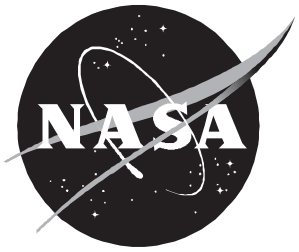

NASA Technical Paper 3466

Application of Two Procedures for Dual-Point Design of Transonic Airfoils

Raymond E. Mineck, Richard L. Campbell, and Dennis O. Allison

September 1994

NASA Technical Paper 3466

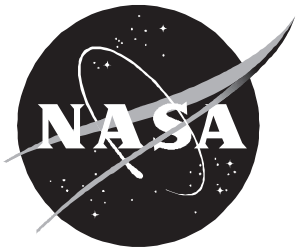

Application of Two Procedures for Dual-Point Design of Transonic Airfoils

Raymond E. Mineck, Richard L. Campbell, and Dennis O. Allison
Langley Research Center • Hampton, Virginia

National Aeronautics and Space Administration
Langley Research Center • Hampton, Virginia 23681-0001

September 1994

This publication is available from the following sources:

NASA Center for AeroSpace Information
800 Elkridge Landing Road
Linthicum Heights, MD 21090-2934
(301) 621-0390

National Technical Information Service (NTIS)
5285 Port Royal Road
Springfield, VA 22161-2171
(703) 487-4650

Abstract

Two dual-point design procedures were developed to reduce the objective function of a baseline airfoil at two design points. The first procedure to develop a redesigned airfoil used a weighted average of the shapes of two intermediate airfoils redesigned at each of the two design points. The second procedure used a weighted average of two pressure distributions obtained from an intermediate airfoil redesigned at each of the two design points. Each procedure was used to design a new airfoil with reduced wave drag at the cruise condition without increasing the wave drag or pitching moment at the climb condition. Two cycles of the airfoil shape-averaging procedure successfully designed a new airfoil that reduced the objective function and satisfied the constraints. One cycle of the target (desired) pressure-averaging procedure was used to design two new airfoils that reduced the objective function and came close to satisfying the constraints.

Introduction

Transport aircraft are typically designed to cruise efficiently at a single flight condition, the cruise design point, while meeting other design constraints. As the result of a myriad of factors such as air traffic control operations, flights behind schedule, and the change in weight as fuel is burned, or other factors, aircraft are often operated at less efficient, off-design flight conditions. The penalty for operating at off-design flight conditions can be significant, especially for wings with supercritical airfoils. Some aircraft, such as the high-speed civil transport, may have two cruise design flight conditions: one for operation over land and the other for operation over water. Aerodynamic performance may be improved if a dual-point design procedure can be developed that considers two design points. Because the steps of a dual-point design procedure for a wing should be similar to those for an airfoil, dual-point design procedures can first be developed for the simpler two-dimensional (2-D) problem and then be extended to the three-dimensional (3-D) problem. Two dual-point design procedures are proposed herein to redesign an airfoil for reduced wave drag at two design points.

Airfoil design codes have been developed that define the airfoil associated with a specified pressure distribution at a single design point. The codes fall into two general categories: inverse methods and predictor/corrector methods. Inverse methods, such as the method described in reference 1, determine the airfoil shape by directly using the velocity distribution on the airfoil surface as a boundary condition. The velocity distribution is derived from the specified surface pressure distribution. Predictor/corrector methods, such as the method described in reference 2, determine the airfoil shape in an iterative process. The predictor module computes the flow field and pressure distribution associated with the current airfoil shape. The corrector module adjusts the airfoil shape to bring the computed and specified pressure distributions into agreement. To ensure that the airfoil shape is practical, constraints on the shape are often included in the corrector module, which can be a numerical optimization technique such as the technique described in reference 3. Numerical optimization techniques search for the minimum value of an objective function subject to constraints. Use of numerical optimization entails a significant increase in the computational time because of the large number of cases that must be evaluated.

Dual-point design capability can be added to predictor/corrector methods that use numerical optimization by adding constraints on the appropriate parameters at the second design point or by including the second design point in the objective function to be minimized. Application of numerical optimization for the dual-point design of an airfoil was demonstrated in reference 4. The goal was to reduce the drag at the maximum operating Mach number without increasing the drag at the maximum range Mach number. The airfoil thickness distribution was constrained such that the original profile had to be contained within the redesigned profile. A simple objective function to minimize the drag at the maximum operating Mach number was defined. The drag at the maximum range Mach number was constrained to be less than that of the baseline airfoil. The results indicated that the goal was achieved. However, satisfying the constraints at the second design point reduced the benefits obtained at the first design point without considering the constraint.

Numerical optimization was used in reference 5 to reduce the drag on an airfoil at two flow conditions. In this case, the objective function was the weighted sum of the drag coefficients at each flow condition. No constraints were imposed on the pitching moment of the redesigned airfoil. Note that the optimum shape is for the set of shape functions used to redesign the airfoil shape and that the optimum shape may not represent the global optimum. Dual-point designs using numerical optimization require a large number of geometries to be evaluated. The number of airfoil geometries that were evaluated in the dual-point design process for the cases studied ranged from 61 to 105. The associated computer resources required to evaluate these geometries is large compared with the resources required for a single-point design without numerical optimization.

Alternative procedures, which require fewer computer resources than current numerical optimization techniques, are desired to redesign an airfoil at more than one design point. A simple multipoint design procedure was used in reference 6 to improve the performance of a cascade at off-design conditions. The procedure analyzed the baseline cascade airfoil at angles of attack from $-3°$ to $3°$ from the design operating condition to obtain the pressure distributions at these two off-design conditions. The two pressure distributions were modified to obtain improved boundary-layer characteristics, and these modified pressure distributions were then used to design two intermediate airfoils, one at each off-design point. The pressure distribution at the design operating condition, which was computed for each of the two intermediate airfoils, was then used to develop a new target (desired) pressure distribution at the design point. This new target pressure distribution was used to design a new airfoil at the design operating condition. This procedure required seven analysis cases and three single-point design cases, significantly fewer than the number of cases processed for the numerical optimization study discussed in reference 5. Results indicated that the new airfoil had better performance than the original airfoil over an angle-of-attack range from $-2°$ to $2°$ from the design operating condition. Although the new airfoil may not be the global optimum, the significant reduction in computer resources makes this type of procedure attractive.

Two dual-point design procedures were proposed in reference 7 that did not require a large number of cases to be processed to define a new airfoil. The two design points are assumed to be sufficiently close to each other that the aerodynamic characteristics at the two design points are similar to each other. Changes in the aerodynamic characteristics are assumed to vary linearly with changes in the airfoil shape. This linear assumption is the underlying basis for the two dual-point design procedures. One procedure used the simple average of the shapes of two intermediate airfoils, with one designed at each design point, to define a new airfoil. The other procedure used the simple average of pressure distributions of two intermediate airfoils to design a new airfoil. Each procedure used the same predictor/corrector airfoil design code. The corrector module included options to constrain the values of certain aerodynamic and geometric characteristics. These procedures required the user to define the "optimum" pressure distribution to be used in the dual-point design process at each design point.

Under a cooperative agreement between NASA and the Cessna Aircraft Company, the dual-point design procedures from reference 7 were used to design a new airfoil, and wind tunnel tests were conducted to verify the results. With user assistance, the two dual-point design procedures were used sequentially to define a redesigned airfoil that had less wave drag at each design point subject to constraints on the pitching moment and the airfoil geometric characteristics. Models of the baseline and the redesigned airfoils were tested in the Langley 0.3-Meter Transonic Cryogenic Tunnel (0.3-m TCT) described in reference 8. Results showed total drag reductions slightly larger than the predicted wave-drag reductions. Details of the tests of the baseline airfoil are presented in reference 9.

Information about the dual-point design procedures, the development of the redesigned airfoil, and the experimental verification of the reduced drag of the redesigned airfoil is included in the appendix of this report. The results indicate that averaging is a viable technique for use in a dual-point design procedure. The good agreement between the computed results and the experimental results indicates that the Euler flow solver with the interactively coupled boundary layer is a suitable mathematical model for the flow fields encountered in this design process. However, the dual-point design procedures of reference 7 had two major drawbacks: the user must define "optimum" pressure distributions, and the simple averaging technique did not necessarily produce the best design. This report describes revised dual-point procedures that eliminate these drawbacks.

The purpose of this report is to describe two revised dual-point design procedures and to demonstrate their application to redesign an airfoil to reduce the value of an objective function specified by

the user. These revised dual-point design procedures, which require significantly fewer cases to be processed than procedures using numerical optimization, should require fewer computer resources. This report presents a description of two revised dual-point design procedures and the associated technique for constrained airfoil design. Application of each modified procedure to a climb condition and to a cruise condition is presented as a practical demonstration for different objective functions.

Symbols

The results are presented in coefficient form with the moment reference center at the quarter-chord. All experimental measurements and calculations were made in U. S. customary units.

C_p local static pressure coefficient, $\frac{p - p_\infty}{q_\infty}$

C_p^* sonic pressure coefficient

c chord, ft

c_d section drag coefficient, $\frac{\text{Drag}}{q_\infty c}$

Δc_d change in section drag coefficient

$c_{d,w}$ section wave-drag coefficient, $\frac{\text{Wave drag}}{q_\infty c}$

c_l section lift coefficient, $\frac{\text{Lift}}{q_\infty c}$

c_m section pitching-moment coefficient, $\frac{\text{Pitching moment}}{q_\infty c^2}$

F objective function

G constraint function

M_∞ free-stream Mach number

p local static pressure, lbf/ft^2

p_∞ free-stream static pressure, lbf/ft^2

q_∞ free-stream dynamic pressure, $\frac{1}{2}\rho_\infty V_\infty^2$, lbf/ft^2

R_c Reynolds number based on chord length, $\frac{\rho_\infty V_\infty c}{\mu_\infty}$

r_{le} leading-edge radius, ft

t local thickness, ft

V_∞ free-stream velocity, ft/sec

W weighting factor

x chordwise distance, positive measured aft from leading edge, ft

y vertical distance, positive measured up from airfoil reference line, ft

α angle of attack, positive leading edge up, deg

μ_∞ free-stream viscosity, slugs/ft-sec

ρ_∞ free-stream density, slugs/ft^3

Subscripts:

f data at foot of shock

max maximum

s shock

1 design point 1

2 design point 2

Abbreviations:

DISC Direct Iterative Surface Curvature

TCT Transonic Cryogenic Tunnel

Airfoil Constrained Design Technique

The constrained design technique of reference 10 was selected for use in this study. This technique designs a new airfoil that produces the desired pressure distribution at the specified flow condition (design point) subject to user-defined constraints. In this study, the new airfoil was subject to the same geometric and aerodynamic constraints that were applied to the design of the baseline airfoil. The technique is divided into three primary parts: a constrained design module to adjust the target (desired) pressure distribution to satisfy the constraints, an airfoil design module to modify the airfoil shape to achieve the target pressure distribution, and an aerodynamic analysis module (flow solver) to compute the pressure distribution associated with the current airfoil shape. These three parts are used in an iterative process to determine the new airfoil shape as shown in figure 1.

The initial airfoil shape and the initial target pressure distribution are input into the computer program to define the current airfoil shape and target pressure distribution. The aerodynamic analysis module then computes the pressure distribution associated with the current airfoil shape. The airfoil design module adjusts the airfoil shape after each iteration to bring the current computed pressure distribution into agreement with the current target pressure distribution. After a specified number of iterations, the constrained design module compares the geometric and aerodynamic characteristics of the

current airfoil shape with the constraints. If any constraints are violated, the constrained design module adjusts the target pressure distribution accordingly. The process is repeated for a user-specified number of design iterations. Efficiency is improved over sequential techniques because the airfoil shape and target pressure distribution converge concurrently. A brief description of the three primary parts of the constrained design technique follows.

The constrained design module modifies the detailed target pressure distribution to eliminate violations of the user-specified constraints. Details of the module are presented in reference 10. The detailed target pressure distribution consists of the target (desired) pressure coefficient at each specified chordwise station. Seven target control points along the chord of each surface of the airfoil are determined to define the major characteristics of the detailed target pressure distribution. Seven was the smallest number of control points required to define reasonably well the acceleration, rooftop, shock, and deceleration regions of the chordwise pressure distribution. A sample of a detailed target pressure distribution and the associated target control points is presented in figure 2. These target control points are adjusted by the constrained design module to satisfy the aerodynamic and geometric constraints. The detailed target pressure distribution is adjusted to match the adjusted target control points. The initial target pressure distribution can be identical to the pressure distribution obtained from the aerodynamic analysis module for the baseline airfoil shape at the specified design point (Mach number, Reynolds number, and section lift coefficient). The user may optionally specify the initial target pressure distribution to achieve specific goals such as reduced adverse pressure gradient or reduced Mach number ahead of the shock.

The constrained design module monitors both the aerodynamic and the geometric constraints. As used in this project, the aerodynamic constraints are the lift coefficient, wave-drag coefficient, pitching-moment coefficient, and the pressure gradient on both surfaces over the forward portion of the airfoil. The geometric constraints are the leading-edge radius, maximum thickness, and local thickness at a specified chordwise location. The constrained design module computes the required aerodynamic and geometric characteristics from the current pressure distribution and from the current airfoil shape. If any constraints are violated, the target control points are adjusted based on empirically derived expressions described in reference 10. In certain instances, the expressions may indicate that a fully constrained target is not possible. In these cases, one or more aerodynamic constraints are relaxed to allow the remaining constraints to be satisfied. The pitching-moment coefficient is relaxed first and the wave-drag coefficient is relaxed second. The adjusted target control points are used to adjust the detailed target pressure distribution.

The airfoil design module utilizes the Direct Iterative Surface Curvature (DISC) method of Campbell and Smith (ref. 2) which designs a new airfoil by iterating the airfoil shape to obtain the target pressure distribution. The airfoil design module compares the computed current pressure distribution associated with the current shape with the detailed target pressure distribution. The difference between the computed current and target pressure distributions at each chordwise location on the airfoil is used to determine the change in the local airfoil surface curvature. The ordinates at all chordwise locations downstream of the curvature change are linearly sheared to obtain the required change in local curvature, as shown in figure 3(a). If the resulting airfoil does not close at the trailing edge, the points on each surface are linearly sheared to form a conventional, closed trailing edge, as shown in figure 3(b). The nose camber line and the airfoil upper and lower surfaces are smoothed. The computational grid is then automatically adjusted to compensate for the change in the airfoil shape.

Since this application could involve flow fields with strong shocks, the Euler equations were selected to model the flow field. The Euler equation solver GAUSS2, which was developed by Hartwich (ref. 11), was used for the aerodynamic analysis module. The code solves the Euler equations, cast in a nonconservative form, on a structured grid using an implicit upwind-differencing procedure. The use of a shock-fitting approach produces sharp shocks, even on relatively coarse grids. In regions away from the shock, a second-order, split-coefficient-matrix upwinding method is used. Convergence to steady state is accelerated by a diagonalized approximate factorization technique. The airfoil lift and pitching-moment coefficients are computed by integrating the chordwise pressure coefficient distribution. Viscous effects have been incorporated into the code by using a boundary-layer displacement-thickness approach. For this study, the boundary-layer characteristics are computed in a separate subroutine by using a modified version of the approach by Stratford and Beavers (ref. 12), and the viscous drag coefficient is estimated by using the technique by Squire and Young (ref. 13). Wave drag is computed from the far-field entropy, based on the approach of Oswatitsch (ref. 14).

Description of Revised Dual-Point Design Procedures

The two dual-point design procedures of reference 7 (also included in the appendix of this report) were revised for use in this study. The revisions eliminated the need for the user to specify an initial improved target pressure distribution and defined a weighted averaging method based on reducing the objective function. The goal of each procedure was to define a redesigned airfoil that, subject to constraints, had a smaller objective function than the baseline airfoil. The objective function could involve aerodynamic and geometric characteristics of the airfoil at more than one design point. Possible constraints include the airfoil leading-edge radius, maximum airfoil thickness, thickness at a chordwise station, pitching moment, and wave drag at either of the design points.

Initial Processing for Each Design Cycle

The first dual-point design procedure uses the weighted average of the ordinates of two intermediate airfoils to define a new airfoil shape, and this procedure will be referred to as "airfoil shape averaging." The second dual-point design procedure uses the weighted average of two pressure distributions to design a new airfoil, and this procedure will be referred to as "target pressure averaging." Each procedure begins with the same initial processing, as shown in figure 4. The baseline airfoil A is analyzed at both design points. The desired aerodynamic and geometric characteristics are specified at each design point for use by the airfoil constrained design technique, that is, the constrained DISC method. This method modifies the pressure distribution from the analysis of the baseline airfoil to achieve the desired aerodynamic and geometric characteristics so that the user is not required to define an improved initial target pressure distribution, as was the case in reference 7. Two intermediate airfoils, designated B and C, are designed, one at each design point, by using the airfoil constrained design technique. The aerodynamic characteristics of each intermediate airfoil, developed at one design point, are analyzed at the other design point. By using these results, the objective function (F) is evaluated for the baseline airfoil and for the two intermediate airfoils.

The objective function is plotted against the weighting factor of one of the airfoils (W), as shown in figure 5. For this example, the objective function for airfoil B is plotted at 1.0 (all of airfoil B and none of airfoil C), and the objective function for airfoil C is plotted at 0 (none of airfoil B and all of airfoil C). The value of the objective function is assumed to vary linearly with the fraction of the airfoil. Constraint functions (G) are also plotted as a fraction of the same airfoil. If none of the constraints are violated, the intermediate airfoil, either B or C, having the lower objective function is the new airfoil. If one or more of the constraints are violated, the weighting factor of airfoil B (W_{B}) that produces the minimum objective function without violating the constraints is selected. This value of the weighting factor is used for the procedures for airfoil shape averaging and target pressure averaging.

Use of the weighting factor results in selecting the smallest value of the objective function for which no constraint violations occur, thus eliminating the drawback of the simple average used in reference 7. In the initial processing, the airfoil constrained design technique developed an intermediate airfoil at each design point that had improved characteristics relative to the baseline airfoil at that particular design point. Changes to the airfoil shape or to the pressure distribution are associated with the improved characteristics, and the weighted average serves as a filter. Similar changes at a chordwise location for both intermediate airfoils will pass through the weighted average and promote those changes in the new airfoil. Opposing changes will cancel part of each other and reduce those changes in the new airfoil. Thus, the new airfoil shape or the new target pressure distribution from the weighted average should contain some of the improvements designed into the intermediate airfoils by the constrained airfoil design technique.

Airfoil Shape Averaging

The airfoil shape-averaging procedure uses a weighted average of the shapes of the two intermediate airfoils to define a new airfoil (D), as shown in figure 4. The procedure begins with the initial processing described previously, shown in the left part of figure 4, which defines two intermediate airfoils. The aerodynamic and geometric characteristics are used to define the values of the objective function and the constraints. These are then used to obtain the weighting factor (W_{B}). The new (redesigned) airfoil D is the weighted average of the shapes of two intermediate airfoils, B and C. At each chordwise location, the ordinate of the redesigned airfoil D is defined by

$$\frac{y}{c}(\mathrm{D}) = W_{\mathrm{B}}\,\frac{y}{c}(\mathrm{B}) + (1 - W_{\mathrm{B}})\,\frac{y}{c}(\mathrm{C})$$

By using the weighted average, some improvements from the constrained DISC method are passed to the averaged airfoil. The aerodynamic characteristics of

the averaged airfoil D are analyzed at both design points. The results are used to evaluate the objective function and to check for any constraint violations. If the objective function for the averaged airfoil is less than the objective function for the baseline airfoil and no violated constraints occur, the dual-point design cycle is complete. To find an airfoil shape closer to the optimum, the new airfoil D becomes the baseline airfoil A, and then the airfoil shape-averaging procedure is repeated by beginning with the initial processing. If the objective function for the new (averaged) airfoil is greater than the objective function for the baseline airfoil, different intermediate airfoils are needed. Less stringent aerodynamic and/or geometric constraints should be specified at each design point for use by the airfoil constrained design technique. Experiences with the procedures suggest that reducing the desired reduction in the wave drag by about half will often alleviate problems in obtaining satisfactory intermediate airfoils. The initial processing is then repeated to define two different intermediate airfoils. The airfoil shape-averaging procedure is repeated by using the different intermediate airfoils.

Airfoil Target Pressure Averaging

The target pressure-averaging procedure uses a weighted average of the pressure distributions of the two intermediate airfoils at one of the design points to define a new target pressure distribution, as shown in figure 6. The procedure begins with the initial processing described previously (see left part of fig. 6) that defines two intermediate airfoils. The aerodynamic and geometric characteristics are used to define the values of the objective function and the constraints. These are then used to obtain the weighting factor (W_{B}). The desired pressure distribution for the new (redesigned) airfoil, either E or F, is the weighted average of the chordwise pressure distributions of the two intermediate airfoils, B and C. At each chordwise location, the desired target pressure distribution of the redesigned airfoil is defined for the first design point by

$$C_{p,1}(\mathrm{E}) = W_{\mathrm{B}}\, C_{p,1}(\mathrm{B}) + (1 - W_{\mathrm{B}})\, C_{p,1}(\mathrm{C})$$

and for the second design point by

$$C_{p,2}(\mathrm{F}) = W_{\mathrm{B}}\, C_{p,2}(\mathrm{B}) + (1 - W_{\mathrm{B}})\, C_{p,2}(\mathrm{C})$$

By using a weighted average of these two intermediate target pressure distributions, effects from the design of both intermediate airfoils are included in the new target pressure distribution.

The new target pressure distribution is the weighted average of the intermediate pressure distributions all along the chord unless shocks are present on both of the intermediate target pressure distributions being averaged. If shocks are present, special processing (shown in fig. 7) is used for the region between the shocks. The new shock location (x_s(E)) will be the weighted average of the shock locations (x_s(B) for the forward shock and x_s(C) for the aft shock) of the two intermediate pressure distributions. Thus,

$$\frac{x_s(\mathrm{E})}{c} = W_{\mathrm{B}} \frac{x_s(\mathrm{B})}{c} + (1 - W_{\mathrm{B}}) \frac{x_s(\mathrm{C})}{c}$$

By using the averaged pressures at the last two chordwise locations ahead of the forward shock, the new pressures from the forward shock location to the new shock location are determined by extrapolation. The new pressure at the foot of the shock ($C_{p,f}$(E)) is the weighted average of pressures at the foot of the forward and aft shocks ($C_{p,f}$(B) and $C_{p,f}$(C), respectively). Thus,

$$C_{p,f}(\mathrm{E}) = W_{\mathrm{B}}\, C_{p,f}(\mathrm{B}) + (1 - W_{\mathrm{B}})\, C_{p,f}(\mathrm{C})$$

The new pressures aft of the foot of the new shock location but upstream of the aft shock location are determined by interpolation.

The new target pressure distribution is used with the constraints to design a new airfoil (either E or F) at the appropriate design point. (See fig. 6.) The new airfoil is analyzed at the other design point. These results are used to evaluate the objective function and to check for any constraint violations. If the new airfoil developed at one design point has a larger objective function or constraint violations occur, the new target pressure distribution at the other design point is used to design a second new airfoil. This new airfoil is also analyzed at the off-design point to check the objective function and the constraints. If the second new airfoil does not reduce the objective function and satisfy the constraints, less stringent aerodynamic and/or geometric constraints should be specified at each design point, and the target pressure-averaging process, including the initial processing, is repeated. If one of the new airfoils reduces the objective function and satisfies the constraints, the design cycle is complete. To find an airfoil closer to the optimum, the new airfoil (either E or F) becomes the baseline airfoil A and the target pressure-averaging procedure is repeated.

Computer Resources

For this study, the design and analysis cases for the dual-point design procedures were run on a Cray

Y-MP computer. One cycle of the airfoil shape averaging requires six analysis cases and two design cases to be run to define a new airfoil. One cycle of the target pressure averaging requires at least five analysis cases and three design cases to be run. The version of the constrained DISC method used required only 712 kilowords of memory for a 161×33 grid. Analysis cases, which were run for typically 5500 cycles of the flow solver with updates for the boundary-layer characteristics every 100 cycles, required about 0.028 sec of CPU time per cycle. The norm of the residual error was generally reduced five orders of magnitude from the initial free-stream solution. Design cases were run until the maximum change in the chordwise pressure distribution between consecutive cycles was below a user-defined threshold (a change less than 0.004 for this study). Design cases typically required from 2000 to 5000 cycles of the flow solver, depending on the number of target pressure modifications required by the constrained design module. The additional time for the computations in the constrained design module led to a negligible change in the average CPU time required per cycle.

Application of Revised Dual-Point Design Procedures

Design Conditions

The revised dual-point design procedures were used to design a new airfoil for two design points, one representing a climb condition and the other representing a cruise condition. The flow conditions for these points are listed in chart A. For all cases considered, the nose-down pitching moment is constrained to that of the baseline airfoil so that trim drag is not a factor. Also, the new airfoil is constrained to have the same leading-edge radius and maximum thickness as the baseline airfoil. Different goals for the dual-point design procedures are selected for the two cases to be studied. For the first case, the selected goal was to reduce the combined wave drag at the two design points (i.e., equal weighting of the points). For the second case, the goal was to reduce the drag at the cruise condition without increasing the wave drag at the climb condition.

The supercritical airfoil used as the baseline airfoil in reference 7 was also used as the baseline airfoil in this study. Design coordinates of this airfoil are listed in table 1. This airfoil has a maximum thickness of $0.115c$ at the $0.307c$ station and a leading-edge radius of $0.016c$. The aerodynamic characteristics of the baseline airfoil were computed using the GAUSS2 flow solver with the interacted boundary layer. All calculations were performed with the boundary-layer

Chart A

Flight condition	Climb	Cruise
M_∞	0.685	0.735
R_c	8.9×10^6	8.9×10^6
c_l	0.850	0.608

transition fixed on both surfaces at $0.05c$. The "C-type" computational grid had 161 chordwise and 33 normal grid points. The far-field boundary was an ellipse extending seven chords in the upstream direction and six chords in the normal direction from the trailing edge. The wake extended downstream 6 chords from the trailing edge, and 14 chordwise points were in the wake. The effect of the airfoil lift was included in the far-field boundary conditions, thus allowing the far-field boundary condition to be brought closer to the airfoil. Computations using this flow solver, presented in reference 11, indicate that this grid is adequate for the required computations.

The baseline airfoil was analyzed at these two design points, and the results are presented in figure 8. A summary of the geometric and aerodynamic characteristics is found in table 2. Note that a significant amount of wave drag occurs at each design point. Two intermediate airfoils were designed, and the aerodynamic characteristics of each airfoil at the two design points are presented in figures 9 and 10. The wave drag of each intermediate airfoil was reduced at its design point and increased at the other design point. Also, an increase occurred in the nose-down pitching-moment coefficient for both intermediate airfoils at the off-design flow condition. A comparison of the intermediate airfoils designed for the climb (airfoil B) and cruise (airfoil C) conditions with the baseline airfoil is presented in figure 11. The leading-edge radius and the maximum thickness of both intermediate airfoils are very close to the values of the baseline airfoil. Except for the forward portion of the airfoil, the changes in the airfoil shapes from the baseline for the two intermediate airfoil shapes are generally opposite each other.

First Case

In some situations, one of the design points will dominate the design process. Reducing the objective function and satisfying the constraints at the dominant design point will lead to an airfoil that also satisfies the constraints at the second design point. The first case is an example of that situation in that the selected goal was to reduce the combined wave drag at the two design points. The objective function for airfoil B, designed at the climb

condition, is higher than that of the baseline airfoil A (0.0065 versus 0.0055). However, the objective function for airfoil C, designed at the cruise condition, is lower than that of the baseline airfoil A (0.0040 versus 0.0055). The pitching moment of airfoil C at the climb condition is only slightly larger than that of the baseline airfoil A. If necessary, the dual-point design process could be repeated using a less negative pitching-moment constraint to achieve the desired value. Thus, the intermediate airfoil C, designed at the cruise condition, is the new airfoil. For this case, only the initial processing common to both procedures was required to define a new airfoil. Because the desire was to demonstrate the procedures, the process was terminated after only the first cycle. To determine if additional reductions in the objective function are possible, the new airfoil becomes the starting airfoil and the dual-point design process is repeated. Note that although this is an improved airfoil, it is not necessarily the "optimum" airfoil.

Second Case

For the second case, the objective was to reduce the wave drag at the cruise condition with the constraint that the wave drag and pitching moment at the climb condition do not increase. The objective function and the constraint on the wave drag at the climb condition are plotted as a function of the fraction of airfoil B in figure 12. With the assumption of a linear variation of the aerodynamic characteristics with the change in shape, the points are connected with a straight line. The value of the objective function for airfoil B (at $W_B = 1$) is greater than that of the baseline airfoil A (cruise $c_{d,w} = 0.0053$ versus $c_{d,w} = 0.0024$), and so it is not acceptable. The constraint at the climb condition is violated (climb $c_{d,w} = 0.0038$ versus $c_{d,w} = 0.0031$) for airfoil C (at $W_B = 0$), and thus it is not acceptable either. Each of the revised dual-point design procedures will be used to produce a new airfoil. As noted earlier, the different characteristics are assumed to vary linearly as the percentage of the airfoil shape. Averaged airfoils with less than 0.26 of airfoil B are eliminated because of the constraint violation ($c_{d,w} > 0.0031$). The minimum value of the objective function achievable without violating the constraints at that point is selected. The weighting factor (W_B) for the dual-point design procedures is 0.26.

The airfoil shape-averaging procedure (fig. 4) was used to define a new airfoil (D) for the second case by using the value of the weighting factor obtained from figure 12. The aerodynamic characteristics of this airfoil are presented in figure 13. At the climb condition, the wave drag and pitching moment of the new airfoil are slightly greater than that of the baseline airfoil. At the cruise condition, the wave-drag coefficient has been reduced from 0.0024 to 0.0010 with no change in the pitching-moment coefficient. The shape of the airfoil redesigned by using airfoil shape averaging is compared with that of the baseline airfoil in figure 14. The new airfoil has the same maximum thickness and almost the same leading-edge radius. Application of just 1 cycle of the airfoil shape-averaging procedure produced an airfoil that reduced the wave drag at the cruise condition but failed to meet the aerodynamic constraints at the climb condition. A second cycle of the airfoil shape-averaging procedure was used to refine the airfoil shape to satisfy the constraints. The shape of this refined airfoil (D_2) is presented in figure 14. The maximum thickness of the refined airfoil is the same as that of the baseline, but the leading-edge radius is slightly smaller than that of the baseline airfoil. The aerodynamic characteristics of the refined airfoil are presented in figure 15. The refined airfoil satisfies all the aerodynamic constraints, but to satisfy the constraints, the objective function (wave drag at cruise) has increased from 0.0010 to 0.0011. Thus, two cycles of airfoil shape averaging successfully redesigned the baseline airfoil.

The values of the objective function and the wave-drag constraint at the climb condition for airfoil D have been plotted in figure 12. Two additional airfoils were defined: X_1 using a weighting factor of 0.50, and X_2 using a weighting factor of 0.75. These airfoils were analyzed, and the values for the objective and constraint functions for each have also been plotted in figure 12. The values indicate that, for this case, the assumption of a linear variation of objective and constraint functions between the two intermediate airfoils, although not exact, is reasonable for the airfoil shape-averaging dual-point design procedure for these conditions.

The target pressure-averaging procedure (fig. 6) was used to define two new airfoils for the second case, one for each design point. The weighting factor was obtained from figure 12. The weighted target pressure distribution for the climb condition was used to produce airfoil E, and the weighted target pressure distribution for the cruise condition was used to produce airfoil F. The aerodynamic characteristics of these two airfoils are presented in figures 16 and 17 for both design points.

For airfoil E, designed at the climb condition, the pitching-moment coefficient was unchanged, but the constraint on the wave-drag coefficient was violated

by 0.0003 at the climb condition. Both the wave-drag and pitching-moment coefficients were reduced at the cruise condition, thus reducing the objective function. For airfoil F, which was designed at the cruise condition, both the wave-drag and pitching-moment coefficients increased slightly at the climb condition. If needed, this small increase could be eliminated by a second design cycle, as was done for airfoil shape averaging. For a practical engineering problem, this would probably not be considered a constraint violation.

The wave-drag and pitching-moment coefficients were reduced at the cruise condition, thus reducing the objective function. A comparison of the shapes of these airfoils with the baseline airfoil is presented in figure 18. Each of the new airfoils has nearly the same maximum thickness and leading-edge radius as the baseline airfoil. The target pressure-averaging procedure produced two airfoils, both of which satisfied the objective function and came close to satisfying the constraints.

The objective and constraint functions for the new airfoils developed using target pressure averaging (airfoils E and F) have been plotted in figure 12. The results indicate that an assumed linear variation between the intermediate airfoils is also reasonable for dual-point design using target pressure averaging for these conditions.

The objective function and the pitching-moment and wave-drag constraints for the baseline airfoil, the intermediate airfoils, and the redesigned airfoils (D_2, E, and F) are compared in figure 19. Airfoil E had a smaller objective function than airfoil F. However, airfoil E also had a minor constraint violation. A trade study is required to determine the better airfoil. The target pressure-averaging procedure had more difficulty in reaching a solution that satisfied the aerodynamic and geometric constraints. For this case, airfoil shape averaging is the preferred procedure for dual-point design.

Concluding Remarks

Two dual-point design procedures to reduce the wave drag of an airfoil at two design points have been proposed. The first procedure to develop a redesigned airfoil used a weighted average of the shape of two intermediate airfoils redesigned at each of the two design points. The second procedure used a weighted average of two pressure distributions obtained from an intermediate airfoil redesigned at each of the two design points. Each procedure was used to design a new airfoil with reduced drag at the cruise condition without increasing the drag at the climb condition. Two cycles of the airfoil shape-averaging procedure successfully designed a new airfoil that reduced the objective function and satisfied the constraints. One cycle of the target pressure-averaging procedure successfully designed two new airfoils that reduced the objective function. However, each airfoil had a minor constraint violation that could be eliminated with additional design cycles. For this study, airfoil shape averaging was the preferred method for dual-point design.

NASA Langley Research Center
Hampton, VA 23681-0001
June 15, 1994

Appendix

Preliminary Dual-Point Design Procedures

Preliminary dual-point design procedures were defined in reference 7. These earlier procedures were applied to redesign an airfoil to reduce the drag at two design points. The baseline airfoil and the redesigned airfoil were tested in a wind tunnel to verify the drag reduction of the redesigned airfoil relative to the baseline. These results indicated that averaging is a viable technique for a dual-point design procedure and that the computer code used to model the flow field does a good job in simulating the experimental flow field. For completeness, the preliminary dual-point design procedures, their application to reduce the drag at two design points, and results from the experimental verification of the improvements are presented in this appendix. These procedures used an early version of the airfoil constrained design technique (the constrained DISC) described in the main section of this report, and thus a description will not be repeated in the appendix.

Description of Preliminary Dual-Point Design Procedures

Two preliminary dual-point design procedures were defined in reference 7. Each procedure used an iterative approach to redesign an airfoil. The first procedure to develop a new airfoil used a weighted average of the shapes of two intermediate airfoils redesigned at each of the two design points. This procedure will be referred to as "airfoil shape averaging." The second procedure used a weighted average of two pressure distributions obtained from an intermediate airfoil redesigned at the same design point. This procedure will be referred to as "target pressure averaging." A description of each of these dual-point design procedures follows.

Airfoil shape averaging. The first dual-point design procedure averages the shapes of two redesigned intermediate airfoils to develop a new airfoil. A schematic of one design cycle of this procedure is presented in figure A1. The starting airfoil is first analyzed to obtain the chordwise pressure distribution at each design point. These pressure distributions are adjusted by the user to define the initial target pressure distributions at each design point. The user-specified adjustments allow a specific characteristic, such as reduced shock strength or reduced adverse pressure gradient, to be included in the design process. Starting from the appropriate initial target pressure distribution, the constrained design technique develops an intermediate airfoil at each design point. A new airfoil is obtained from the simple average of the shapes of the two intermediate airfoils. The new airfoil is analyzed at both design points, and if the results are not satisfactory, the new airfoil becomes the starting airfoil and the process is repeated. This procedure can be expanded to more than two design points by simply adding additional processing paths for additional design points and defining a suitable weighting function for the averaging of the intermediate airfoil shapes.

Airfoil target pressure averaging. To develop an improved airfoil, the second dual-point design procedure averages the detailed target pressure distributions developed in the iterative process rather than the airfoil shapes. A schematic of the initialization and one design cycle is presented in figure A2. The starting airfoil is first analyzed to obtain the chordwise pressure distributions at each of the design points. The pressure distributions from the analysis are adjusted to define the initial target pressure distributions at each design point. The initialization can start with either design point, and subsequent design cycles will use alternating design points. For this example, design point 1 was selected to start the process. The adjusted target pressure distribution at design point 1 is used with the constraints to design the first intermediate airfoil. The analysis of the starting airfoil, the definition of the initial target pressure distributions, and the design of the first intermediate airfoil constitute the initialization of the process.

The initialization is followed by multiple airfoil design cycles. The latest intermediate airfoil is analyzed to obtain the pressure distribution at each design point. These pressure distributions are used as intermediate target pressure distributions for each design point. The last two intermediate target pressure distributions for the design point are averaged to define the next target pressure distribution, and this averaged distribution is then used with the constraints to design the next intermediate airfoil. The analysis of an intermediate airfoil, the averaging of the last two intermediate target pressure distributions, and the design of the next intermediate airfoil constitute one airfoil design cycle. The intermediate airfoil is analyzed at both design points. If the results are not satisfactory, the airfoil design cycle is repeated at the other design point to develop the next intermediate airfoil. The airfoil design cycle is repeated at alternate design points as needed.

Application of Preliminary Dual-Point Design Procedures

A supercritical airfoil shape was selected as the baseline airfoil (A) for this study, and design

coordinates are listed in table 1. This airfoil has a maximum thickness of $0.115c$ at the $0.307c$ station and a leading-edge radius of $0.016c$. The baseline airfoil aerodynamic characteristics were computed using the GAUSS2 flow solver with the interacted boundary layer. All calculations were performed with the boundary-layer transition fixed on both surfaces at $0.05c$. Two design points were selected: one representing a long-range cruise condition and the other representing a high-speed cruise condition. The flow conditions for these points are listed in chart B. Results from the analysis of the baseline airfoil at these design points are presented in figure A3, and a summary of the geometric and aerodynamic characteristics is found in table 3.

Chart B

Cruise condition	Long range	High speed
M_∞	0.654	0.735
R_c	4.5×10^6	8.9×10^6
c_l	0.979	0.508

The preliminary versions of the procedures for airfoil shape averaging and target pressure averaging were applied in an attempt to redesign the baseline airfoil. The objective function was the sum of the wave drag at the two design points. The section lift, wave drag, and pitching-moment coefficients from the baseline airfoil were used as the aerodynamic constraints on the design of the improved airfoils. The pitching-moment-coefficient constraint was a one-sided constraint in that the pitching-moment coefficient of the new airfoil could not be more negative than the pitching-moment coefficient of the baseline airfoil. Similarly, the wave-drag coefficient of the new airfoil could not be greater than the wave drag of the baseline airfoil. The leading-edge radius, maximum thickness, and thickness at the $0.85c$ location of the baseline airfoil were used as the geometric constraints. In general, the constraint on the local thickness at $0.85c$ did not impact the design process, and thus it will not be discussed herein.

By using airfoil shape averaging, an intermediate airfoil was designed at each design point and was analyzed at the other design point. The aerodynamic results (presented in figs. A4 and A5) indicate that even though each intermediate airfoil had less wave drag than the baseline airfoil at the particular design point, it had a higher wave drag than the baseline airfoil at the other design point, thus violating one of the constraints. The value of the objective function for each of the intermediate airfoils was larger than that of the baseline airfoil. A comparison of the two intermediate airfoil shapes with the baseline airfoil shape (presented in fig. A6) shows that changes in shape for the two intermediate airfoils relative to the baseline were generally in opposition to each other.

The preliminary procedures of airfoil shape averaging and target pressure averaging that used simple averaging could not design a new airfoil that satisfied all the constraints and that significantly reduced the sum of the wave-drag coefficients at the two design points. To develop a new airfoil, the design space was temporarily expanded to see if an alternate path could be found around the boundary posed by the constraints. The preliminary version of the target pressure-averaging procedure was used with relaxed constraints to develop an airfoil with reduced wave drag at both design points. The preliminary version of the airfoil shape-averaging procedure was then used to refine the shape to satisfy all constraints.

Target pressure averaging was used with relaxed constraints to design a series of intermediate airfoils. The leading-edge-radius constraint was eliminated and the pitching-moment constraint was relaxed to -0.077 for the long-range cruise point. The design value for the wave-drag coefficient was 0.0010 for the long-range cruise point and 0.0001 for the high-speed cruise point. The baseline pressure distributions from figure A3 were modified to reduce the Mach number (negative pressure coefficient) just ahead of the shock. The modified pressure distributions became the initial target pressure distributions for the target pressure-averaging procedure. Several iterations of the preliminary target pressure-averaging procedure were used to define a series of intermediate airfoils. The fifth intermediate airfoil showed a significant reduction in the wave drag at the long-range cruise design point without a significant increase at the high-speed cruise design point. This airfoil satisfied the maximum thickness constraint. However, the design process reduced the leading-edge radius from $0.016c$ to $0.005c$. Also, the negative pitching moment exceeded the constrained value at both design points. This airfoil must be redesigned to increase the leading-edge radius and to reduce the negative pitching-moment coefficient.

The airfoil shape-averaging procedure was used with the full set of constraints to redesign the airfoil with the reduced leading-edge radius. The aerodynamic characteristics of the redesigned airfoil are presented in figure A7. Relative to the baseline airfoil, wave drag has been reduced at both design points. The pitching moment was close to the constrained value. At the long-range cruise point, the Mach number ahead of the shock has been reduced

and the loading on the forward portion of the lower surface has been increased.

Figure A8 presents a comparison of the shapes of the baseline airfoil and redesigned airfoil. The maximum thickness and leading-edge radius of the redesigned airfoil are close to the values of the baseline airfoil. Coordinates of the redesigned airfoil are presented in table 4. Through the sequential application of the two preliminary dual-point design procedures, a redesigned airfoil was developed that, for practical purposes, does not have any violations of the geometric or aerodynamic constraints and that reduces the wave drag at both design points.

Experimental Verification of Redesigned Airfoil

Two airfoil models were built, one incorporating the baseline airfoil shape and the other incorporating the redesigned airfoil shape. Each model was tested in the Langley 0.3-meter TCT with the 13- by 13-in. two-dimensional adaptive-wall test section installed in the circuit. (See ref. 8.) The 0.3-m TCT is a fan-driven, cryogenic pressure tunnel that uses nitrogen as a test gas. It can test airfoil models over a Mach number range from about 0.20 to 0.95 at chord Reynolds numbers up to about 50×10^6, based on a model chord of 6 in.

The models used in these tests had a 6-in. chord, and both airfoil models were tested with transition strips placed at the 5-percent-chord location on both surfaces of the model. Details of the experimental tests of the baseline airfoil model are reported in reference 9. A comparison of the experimental and calculated chordwise pressure distributions is presented in figure A9 for the baseline airfoil and in figure A10 for the redesigned airfoil. In general, the pressures are in good agreement. However, the calculated shock location is usually upstream of the measured location and the calculated trailing-edge pressure is more positive than the measured value. This can be attributed to the very simple boundary-layer model used for this study. Overall, the agreement indicates that the flow solver with the simple boundary layer does a good job in simulating the experimental flow field.

A comparison of the measured chordwise pressure distributions for both airfoils at test conditions close to the two design points is presented in figure A11. At both design points, the loading has been increased on the lower surface over the front portion of the redesigned airfoil, and the negative pressure coefficient on the upper surface just ahead of the shock has been reduced. These changes are similar to those found in the computed results presented in figure A7. A comparison of the experimental integrated force and moment coefficients for the two airfoils is presented in figure A12. The redesigned airfoil reduced the drag coefficient by 0.0022 at the long-range cruise condition ($M_\infty = 0.654$) and reduced the drag coefficient by 0.0005 at the high speed cruise condition ($M_\infty = 0.735$). At each design point, little difference occurs in the pitching-moment coefficients between the baseline and the redesigned airfoils. Because the drag reductions at $M_\infty = 0.654$ are even larger at values of c_l above the design value, the redesigned airfoil probably has a larger buffet margin than the baseline airfoil. These drag reductions include not only changes in the wave drag but also changes in the skin friction and pressure drag. At both the long-range cruise point and the high-speed cruise point, the experimental reduction in the total drag coefficient (fig. A12) was slightly larger than the calculated reduction in the wave-drag coefficient (fig. A7).

The agreement of the experimental results and the calculations for the pressure coefficients indicates that the flow solver with the interacted boundary layer is suitable for modeling the flow fields for the design conditions studied. The agreement of the predicted wave-drag reduction and the measured total drag reduction indicates that averaging is a viable concept for a dual-point design procedure.

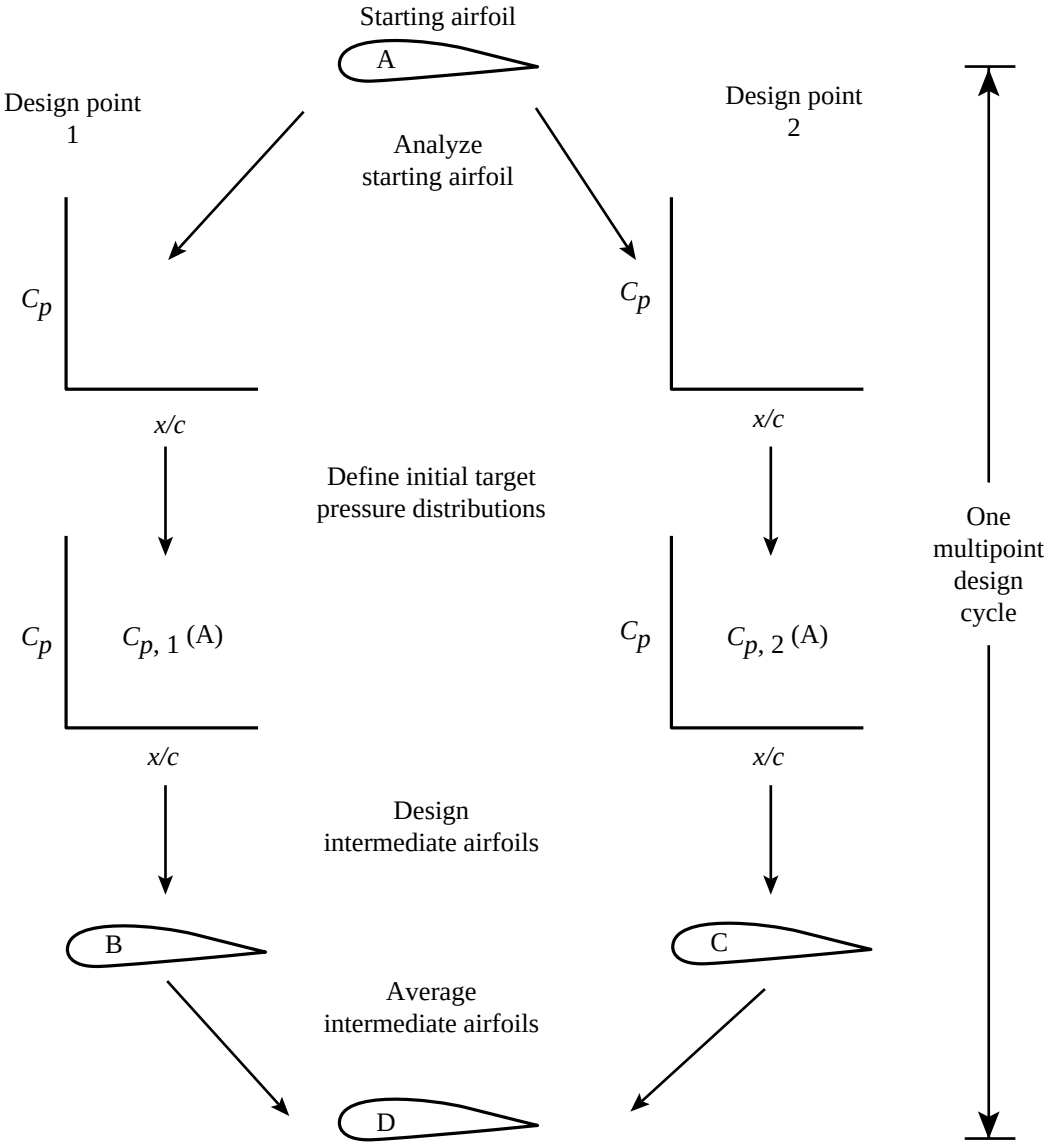

Figure A1. Preliminary version of multipoint design procedure using airfoil shape averaging.

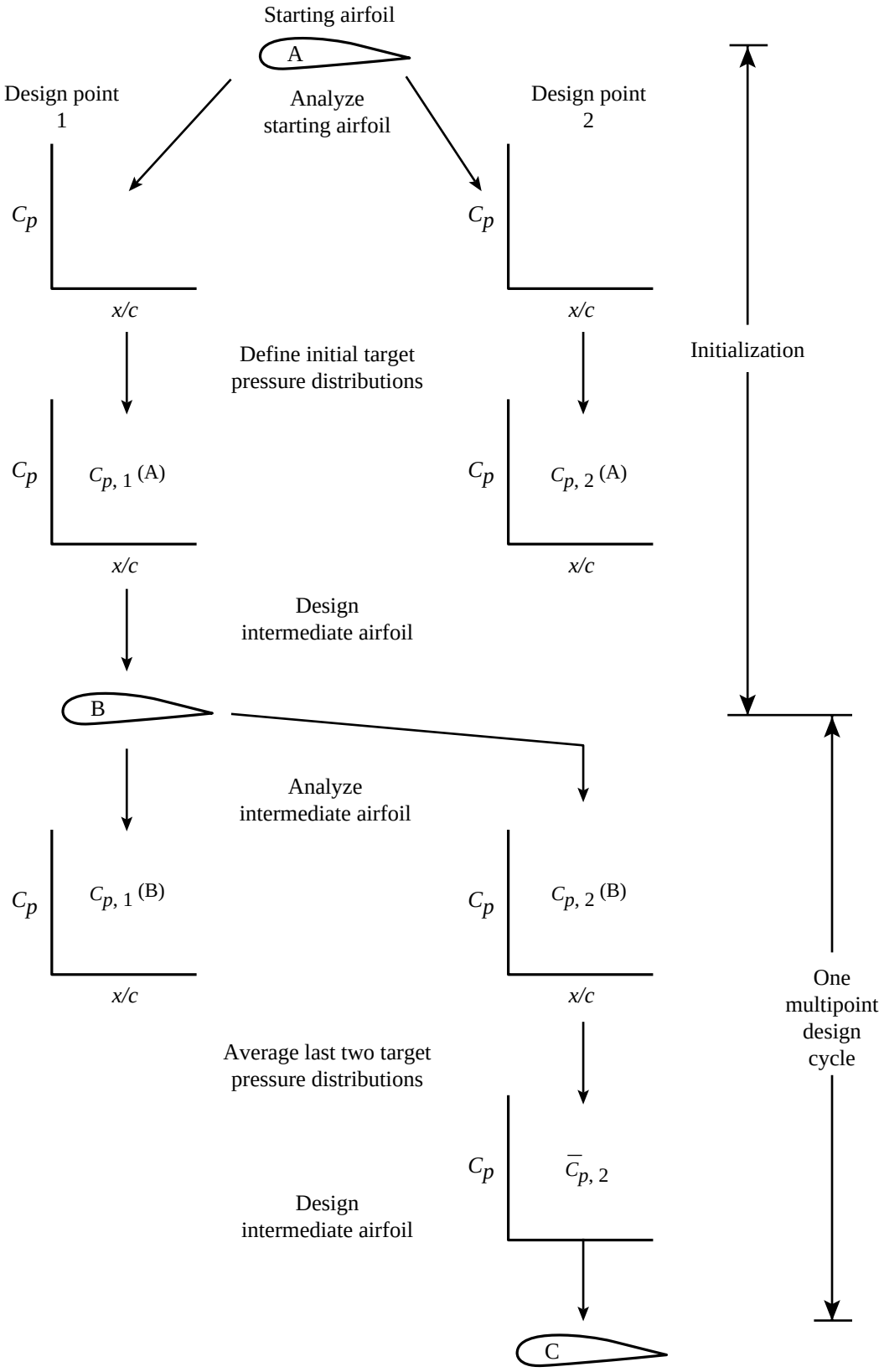

Figure A2. Preliminary version of multipoint design procedure using target pressure averaging. $\overline{C}_{p,2}$ denotes average of two target pressure distributions.

References

1. Volpe, G.; and Melnik, R. E.: A Method for Designing Closed Airfoils for Arbitrary Supercritical Speed Distributions. AIAA-85-5023, Oct. 1985.

2. Campbell, Richard L.; and Smith, Leigh A.: A Hybrid Algorithm for Transonic Airfoil and Wing Design. *A Collection of Technical Papers—AIAA 5th Applied Aerodynamics Conference*, Aug. 1987, pp. 527–538. (Available as AIAA-87-2552.)

3. Vanderplaats, Garret N.: *Approximation Concepts for Numerical Airfoil Optimization.* NASA TP-1370, 1979.

4. Hinson, M. L.: A Series of Airfoils Designed by Transonic Drag Minimization for Gates Learjet Aircraft. *Transonic Aerodynamics*, David Nixon, ed., AIAA, 1982, pp. 489–509.

5. Hager, J. O.; Eyi, S.; and Lee, K. D.: Multi-Point Design of Transonic Airfoils Using Optimization. AIAA-92-4225, Aug. 1992.

6. Schmidt, E.; and Klimetzek, F.: Inverse Computation of Transonic Internal Flows With Application for Multi-Point-Design of Supercritical Compressor Blades. *Computational Methods for Aerodynamic Design (Inverse) and Optimization*, AGARD-CP-463, 1990, pp. 11-1–11-13.

7. Mineck, Raymond E.; and Campbell, Richard L.: Demonstration of Multipoint Design Procedures for Transonic Airfoils. AIAA-93-3114, July 1993.

8. Mineck, Raymond E.; and Hill, Acquilla S.: *Calibration of the 13- by 13-Inch Adaptive Wall Test Section for the Langley 0.3-Meter Transonic Cryogenic Tunnel.* NASA TP-3049, 1990.

9. Allison, Dennis O.; and Mineck, Raymond E.: *Aerodynamic Characteristics and Pressure Distributions for an Executive-Jet Baseline Airfoil Section.* NASA TM-4529, 1993.

10. Campbell, Richard L.: *An Approach to Constrained Aerodynamic Design With Application to Airfoils.* NASA TP-3260, 1992.

11. Hartwich, Peter M.: Fresh Look at Floating Shock Fitting. *AIAA J.*, vol. 29, no. 7, July 1991, pp. 1084–1091.

12. Stratford, B. S.; and Beavers, G. S.: *The Calculation of the Compressible Turbulent Boundary Layer in an Arbitrary Pressure Gradient—A Correlation of Certain Previous Methods.* R. & M. No. 3207, British Aeronaut. Res. Coun., 1961.

13. Squire, H. B.; and Young, A. D.: *The Calculation of the Profile Drag of Aerofoils.* R. & M. No. 1838, British Aeronaut. Res. Coun., 1938.

14. Oswatitsch, Klaus (English version by Gustav Kuerti): *Gas Dynamics.* Volume I of *Applied Mathematics and Mechanics*, Academic Press, Inc., 1956, pp. 447–497.

Table 1. Design Coordinates of Baseline Airfoil

x/c	Values of y/c for—	
	Upper surface	Lower surface
0.00000	0.00000	0.00000
0.00099	0.00635	−0.00489
0.00301	0.01117	−0.00821
0.00604	0.01562	−0.01132
0.01005	0.01974	−0.01431
0.01500	0.02362	−0.01702
0.02088	0.02731	−0.01949
0.02764	0.03076	−0.02183
0.03528	0.03395	−0.02407
0.04374	0.03692	−0.02622
0.05302	0.03969	−0.02830
0.06308	0.04230	−0.03035
0.07389	0.04477	−0.03234
0.08543	0.04713	−0.03428
0.09766	0.04937	−0.03617
0.11056	0.05152	−0.03797
0.12411	0.05358	−0.03968
0.13826	0.05554	−0.04126
0.15300	0.05740	−0.04270
0.16830	0.05915	−0.04400
0.18413	0.06078	−0.04512
0.20045	0.06228	−0.04605
0.21725	0.06364	−0.04680
0.23450	0.06484	−0.04735
0.25216	0.06587	−0.04769
0.27021	0.06674	−0.04783
0.28863	0.06743	−0.04777
0.30737	0.06796	−0.04751
0.32642	0.06831	−0.04705
0.34575	0.06851	−0.04642
0.36533	0.06854	−0.04561
0.38513	0.06840	−0.04465
0.40512	0.06809	−0.04355
0.42527	0.06760	−0.04233
0.44557	0.06691	−0.04100
0.46597	0.06601	−0.03958
0.48646	0.06488	−0.03808
0.50699	0.06353	−0.03651
0.52756	0.06197	−0.03487
0.54812	0.06020	−0.03317
0.56865	0.05826	−0.03141
0.58912	0.05617	−0.02961
0.60950	0.05397	−0.02777
0.62977	0.05168	−0.02591
0.64990	0.04933	−0.02403
0.66986	0.04692	−0.02214
0.68962	0.04448	−0.02027
0.70915	0.04200	−0.01842
0.72843	0.03948	−0.01662
0.74742	0.03694	−0.01489
0.76611	0.03438	−0.01324
0.78445	0.03181	−0.01170
0.80243	0.02922	−0.01028
0.82002	0.02665	−0.00897
0.83718	0.02409	−0.00781
0.85389	0.02157	−0.00678
0.87013	0.01910	−0.00591
0.88585	0.01670	−0.00520
0.90105	0.01438	−0.00463
0.91568	0.01217	−0.00423
0.92972	0.01006	−0.00397
0.94314	0.00807	−0.00385
0.95592	0.00621	−0.00386
0.96802	0.00447	−0.00398
0.97942	0.00285	−0.00421
0.99009	0.00136	−0.00453
1.00000	0.00000	−0.00490

Table 2. Geometric and Aerodynamic Characteristics of Baseline Airfoil at Climb and Cruise Design Conditions

Design conditions	Climb	Cruise
M_∞	0.685	0.735
R_c	8.9×10^6	8.9×10^6
α, deg . . .	2.88	1.17
c_l	0.850	0.608
$c_{d,w}$	0.0031	0.0024
c_m	-0.060	-0.079
x_s/c	0.35	0.48
r_{le}/c	0.016	0.016
$t_{\max}/c$ . . .	0.115	0.115

Table 3. Geometric and Aerodynamic Characteristics of Baseline Airfoil at Long-Range and High-Speed Cruise Design Conditions

Cruise conditions	Long range	High speed
M_∞	0.654	0.735
R_c	4.5×10^6	8.9×10^6
α, deg . . .	4.37	0.69
c_l	0.979	0.508
$c_{d,w}$	0.0042	0.0007
c_m	-0.054	-0.077
x_s/c	0.23	0.44
r_{le}/c	0.016	0.016
$t_{\max}/c$ . . .	0.115	0.115

Table 4. Design Coordinates of Redesigned Airfoil

x/c	Values of y/c for—	
	Upper surface	Lower surface
0.00000	0.00000	0.00000
0.00099	0.00619	−0.00601
0.00301	0.01045	−0.00987
0.00604	0.01431	−0.01315
0.01005	0.01788	−0.01594
0.01500	0.02122	−0.01832
0.02088	0.02438	−0.02035
0.02764	0.02740	−0.02210
0.03528	0.03030	−0.02362
0.04374	0.03307	−0.02496
0.05302	0.03570	−0.02617
0.06308	0.03817	−0.02732
0.07389	0.04048	−0.02847
0.08543	0.04269	−0.02967
0.09766	0.04480	−0.03096
0.11056	0.04685	−0.03235
0.12411	0.04881	−0.03386
0.13826	0.05068	−0.03546
0.15300	0.05248	−0.03714
0.16830	0.05419	−0.03888
0.18413	0.05585	−0.04063
0.20045	0.05743	−0.04235
0.21725	0.05891	−0.04400
0.23450	0.06025	−0.04554
0.25216	0.06145	−0.04692
0.27021	0.06246	−0.04812
0.28863	0.06328	−0.04911
0.30737	0.06391	−0.04988
0.32642	0.06437	−0.05041
0.34575	0.06466	−0.05069
0.36533	0.06481	−0.05072
0.38513	0.06483	−0.05049
0.40512	0.06475	−0.04999
0.42527	0.06458	−0.04922

x/c	Values of y/c for—	
	Upper surface	Lower surface
0.44557	0.06430	−0.04819
0.46597	0.06390	−0.04692
0.48646	0.06331	−0.04541
0.50699	0.06251	−0.04369
0.52756	0.06147	−0.04178
0.54812	0.06018	−0.03969
0.56865	0.05865	−0.03744
0.58912	0.05689	−0.03506
0.60950	0.05492	−0.03257
0.62977	0.05277	−0.02999
0.64990	0.05046	−0.02735
0.66986	0.04802	−0.02469
0.68962	0.04546	−0.02204
0.70915	0.04282	−0.01945
0.72843	0.04012	−0.01695
0.74742	0.03738	−0.01459
0.76611	0.03462	−0.01240
0.78445	0.03186	−0.01042
0.80243	0.02913	−0.00867
0.82002	0.02643	−0.00718
0.83718	0.02380	−0.00594
0.85389	0.02125	−0.00496
0.87013	0.01880	−0.00423
0.88585	0.01646	−0.00372
0.90105	0.01423	−0.00342
0.91568	0.01212	−0.00329
0.92972	0.01011	−0.00330
0.94314	0.00822	−0.00343
0.95592	0.00641	−0.00365
0.96802	0.00469	−0.00392
0.97942	0.00305	−0.00423
0.99009	0.00149	−0.00456
1.00000	0.00000	−0.00489

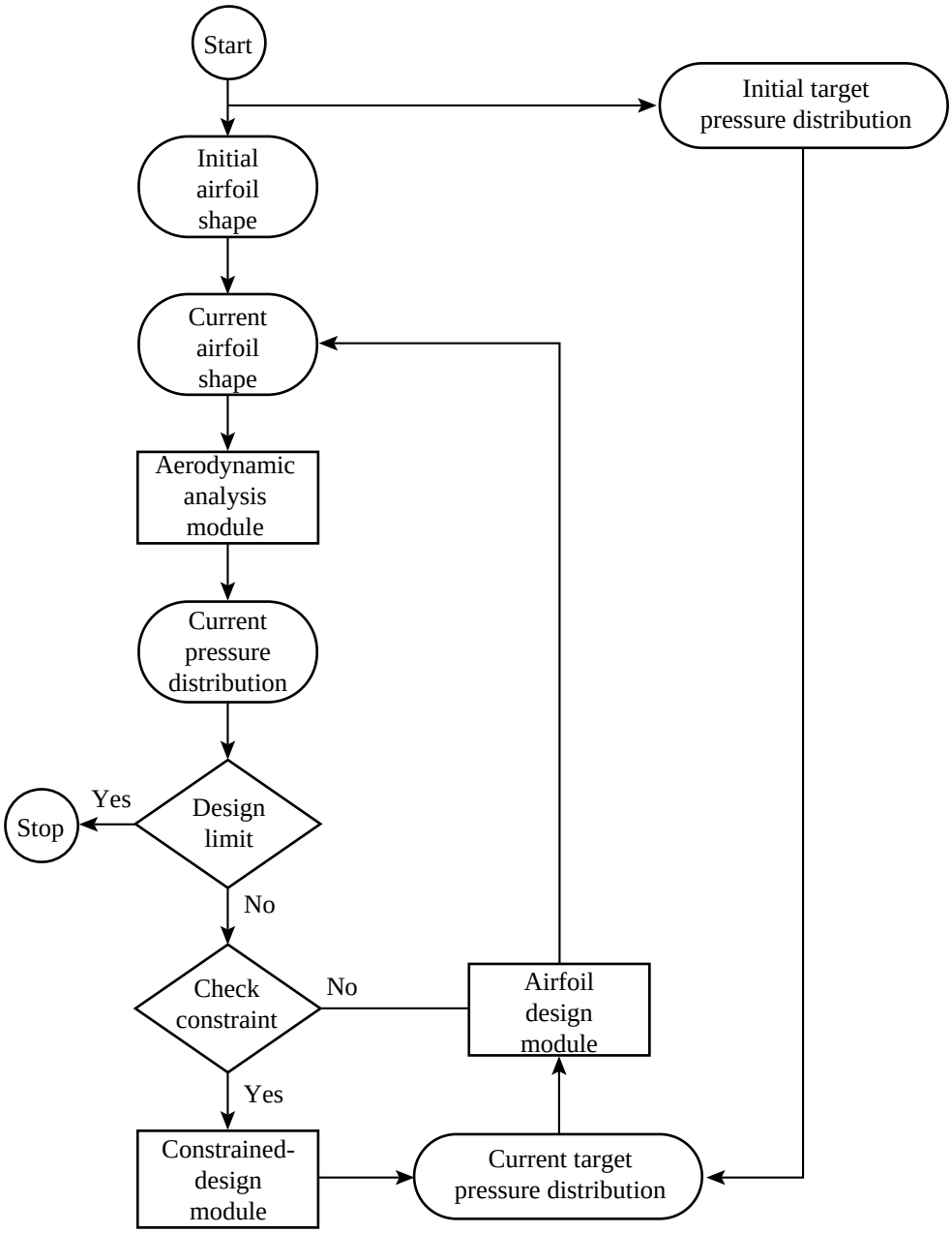

Figure 1. Processing for constrained-design technique of airfoil.

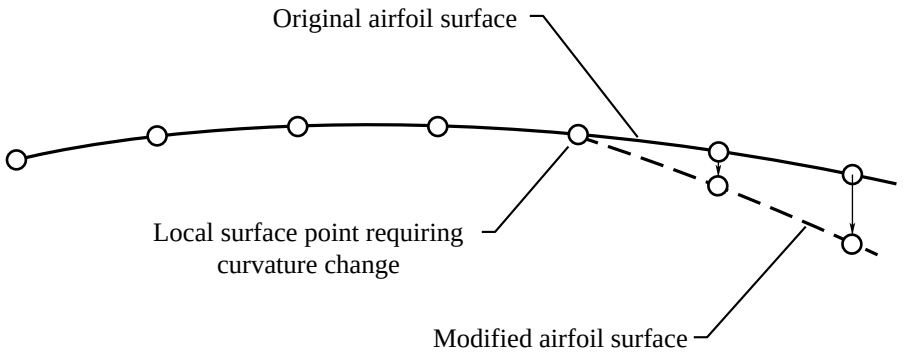

(a) Modification of surface shape for curvature change.

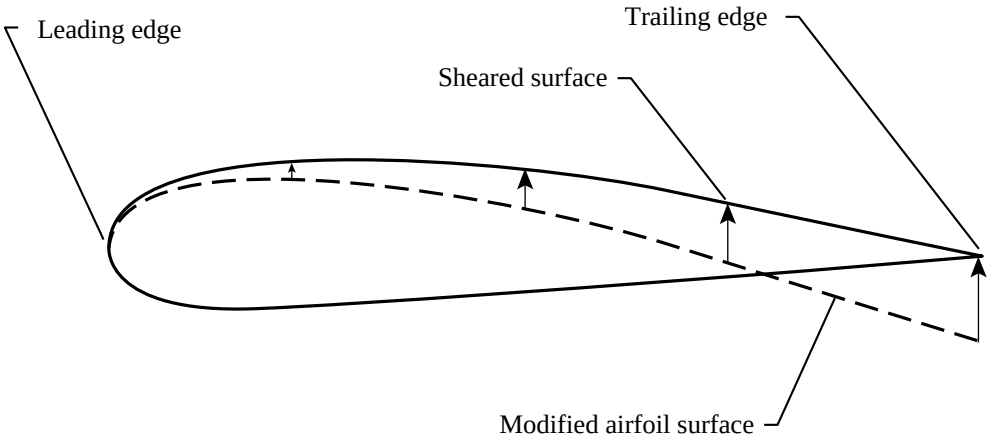

(b) Surface shearing to close trailing edge.

Figure 3. Modification of airfoil shape for change in surface curvature.

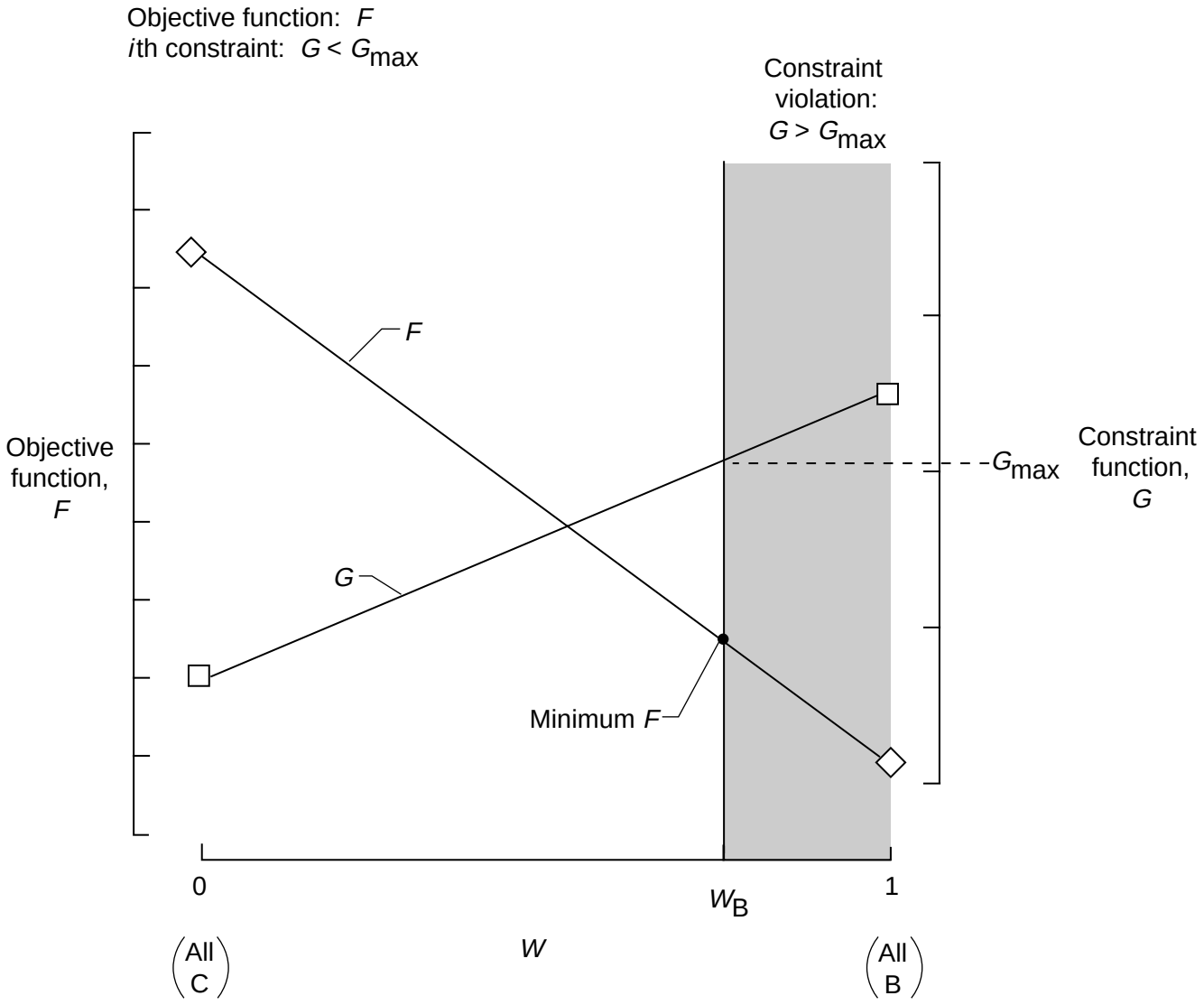

Figure 5. Determination of weighting factor (W) for objective function (F) with constraint function (G).

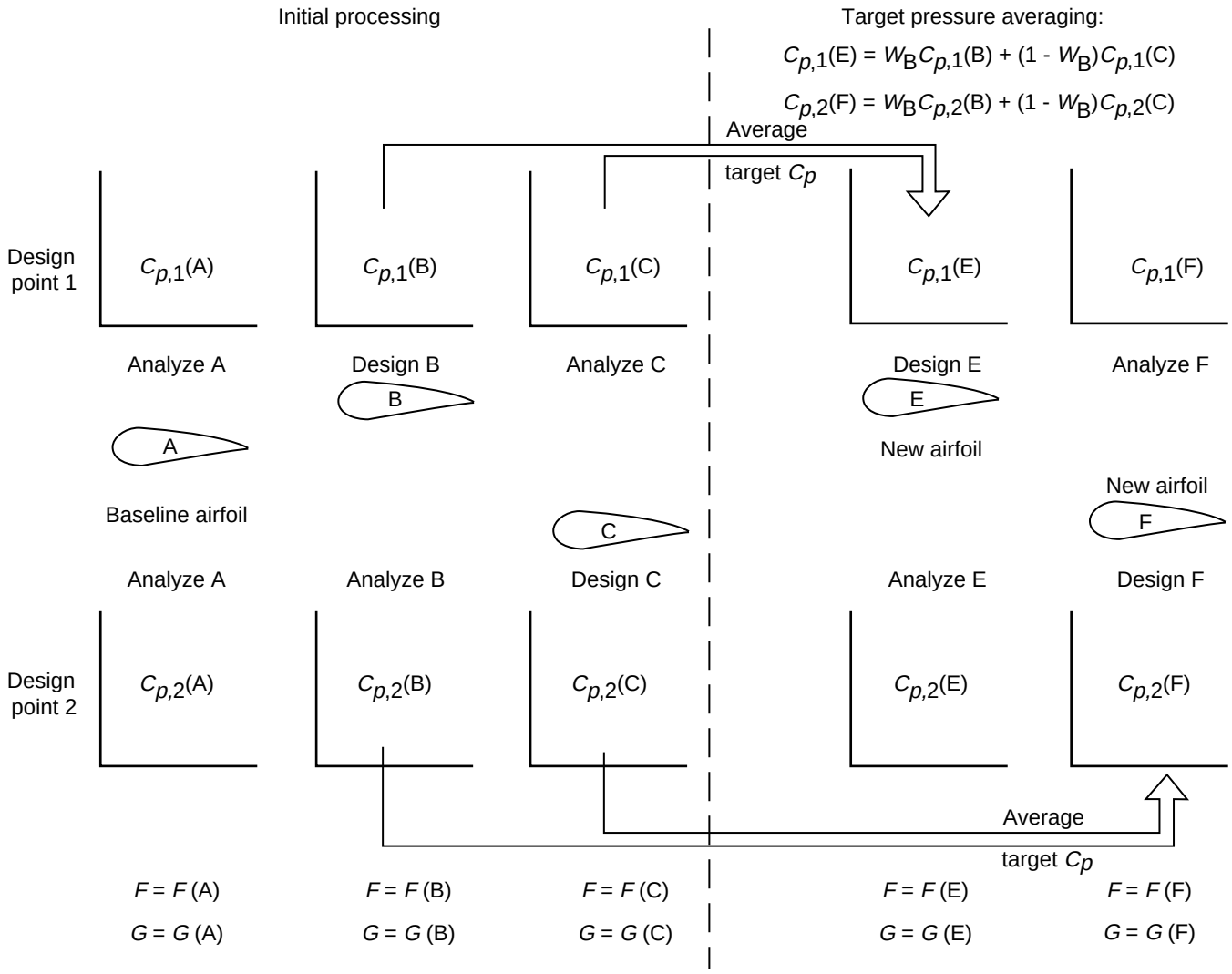
Initial processing
Target pressure averaging:
$C_{p,1}(E) = W_B C_{p,1}(B) + (1 - W_B) C_{p,1}(C)$
$C_{p,2}(F) = W_B C_{p,2}(B) + (1 - W_B) C_{p,2}(C)$
Average
target C_p
Design point 1
$C_{p,1}(A)$
$C_{p,1}(B)$
$C_{p,1}(C)$
$C_{p,1}(E)$
$C_{p,1}(F)$
Analyze A
Design B
Analyze C
Design E
Analyze F
B
E
A
New airfoil
New airfoil
Baseline airfoil
C
F
Analyze A
Analyze B
Design C
Analyze E
Design F
Design point 2
$C_{p,2}(A)$
$C_{p,2}(B)$
$C_{p,2}(C)$
$C_{p,2}(E)$
$C_{p,2}(F)$
Average
target C_p
$F = F(A)$
$F = F(B)$
$F = F(C)$
$F = F(E)$
$F = F(F)$
$G = G(A)$
$G = G(B)$
$G = G(C)$
$G = G(E)$
$G = G(F)$

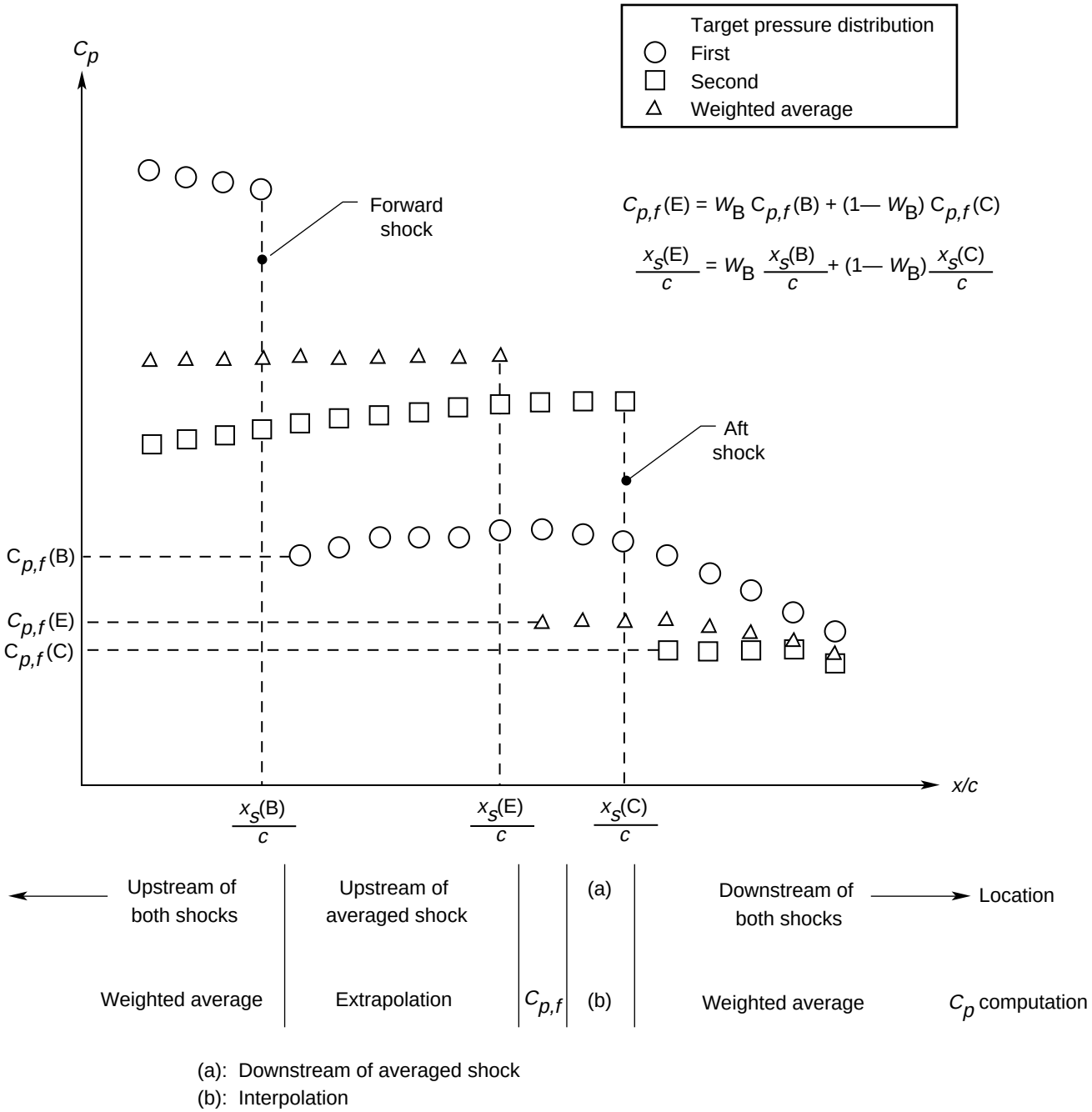

Figure 7. Weighted averaging of target pressure distributions when shocks are present.

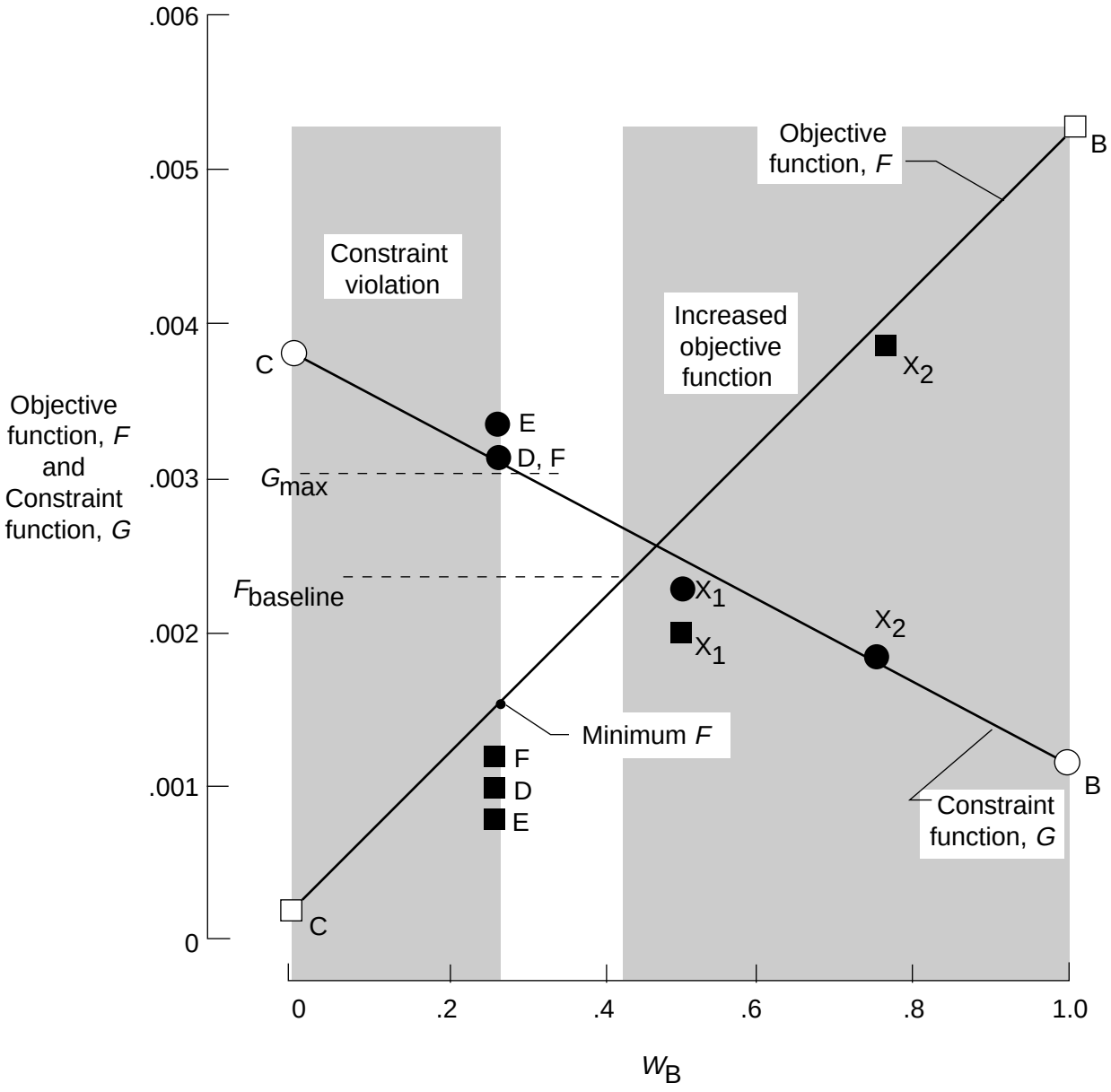

Figure 12. Determination of weighting factor for multipoint procedures. Solid symbols with letter denote new airfoils.

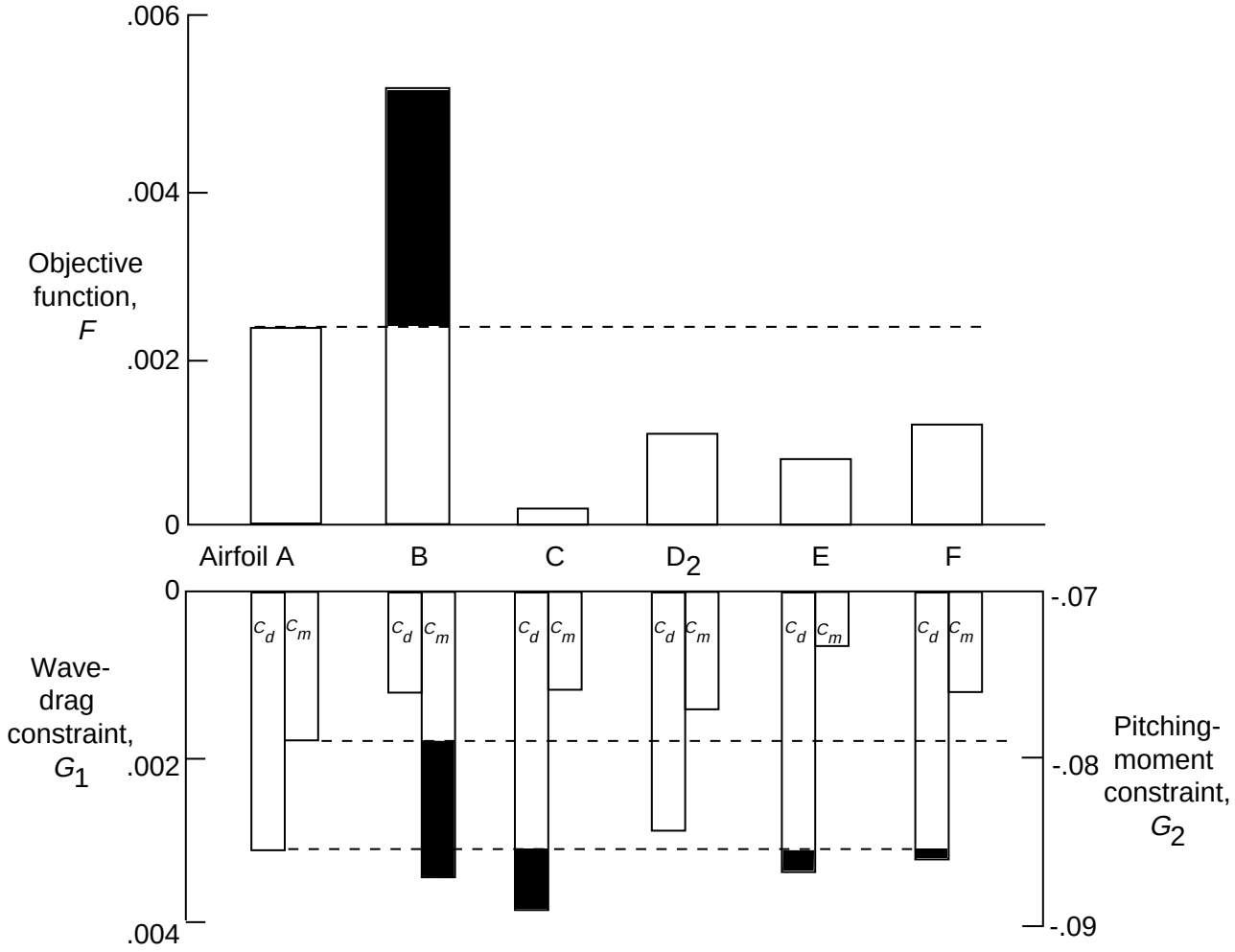

Figure 19. Comparison of objective function and constraint functions of baseline, intermediate, and new airfoils.

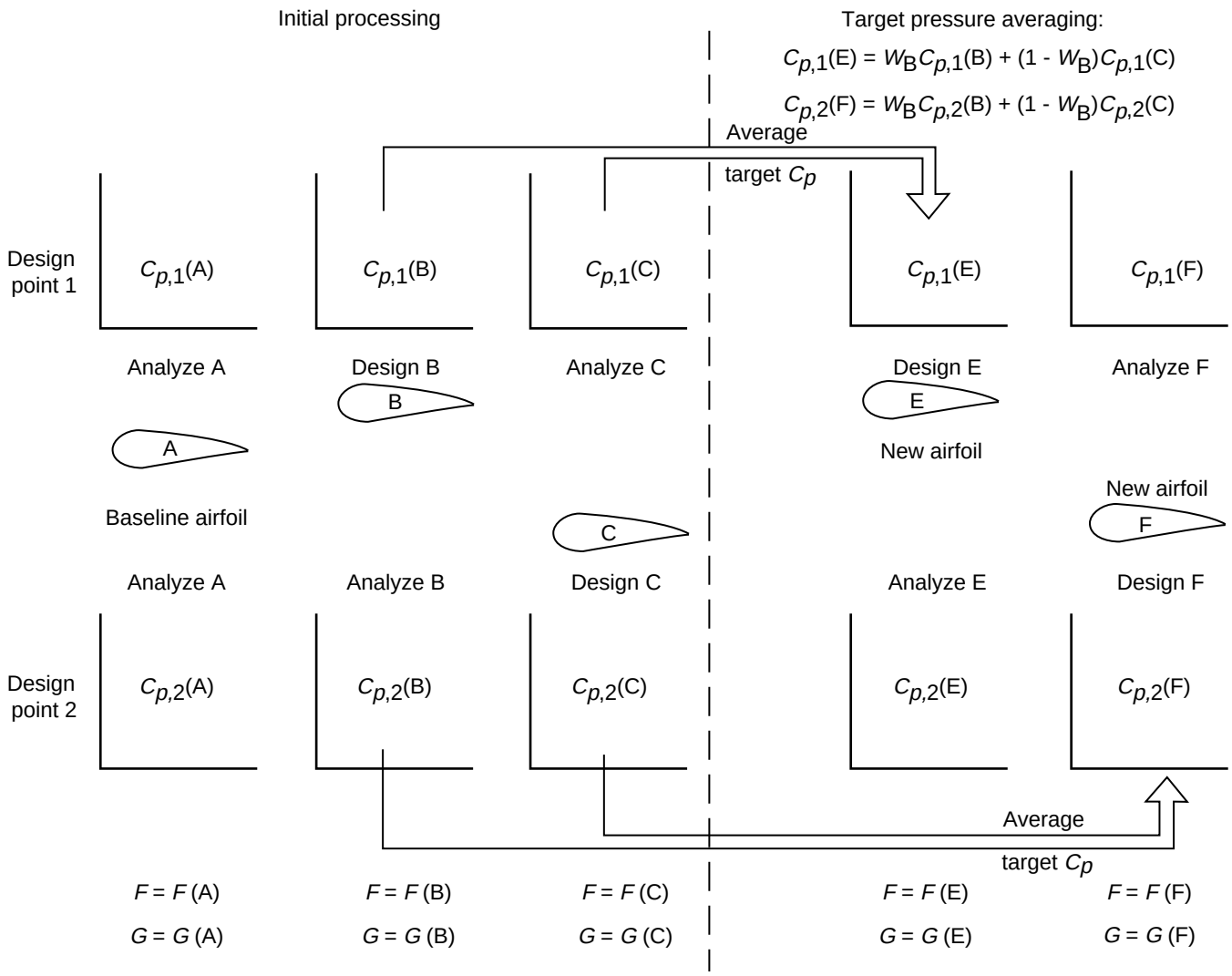
Initial processing
Target pressure averaging:
$C_{p,1}(E) = W_B C_{p,1}(B) + (1 - W_B) C_{p,1}(C)$
$C_{p,2}(F) = W_B C_{p,2}(B) + (1 - W_B) C_{p,2}(C)$
Average
target C_p
Design point 1
$C_{p,1}(A)$
$C_{p,1}(B)$
$C_{p,1}(C)$
$C_{p,1}(E)$
$C_{p,1}(F)$
Analyze A
Design B
Analyze C
Design E
Analyze F
B
E
A
New airfoil
New airfoil
Baseline airfoil
C
F
Analyze A
Analyze B
Design C
Analyze E
Design F
Design point 2
$C_{p,2}(A)$
$C_{p,2}(B)$
$C_{p,2}(C)$
$C_{p,2}(E)$
$C_{p,2}(F)$
Average
target C_p
$F = F(A)$
$F = F(B)$
$F = F(C)$
$F = F(E)$
$F = F(F)$
$G = G(A)$
$G = G(B)$
$G = G(C)$
$G = G(E)$
$G = G(F)$

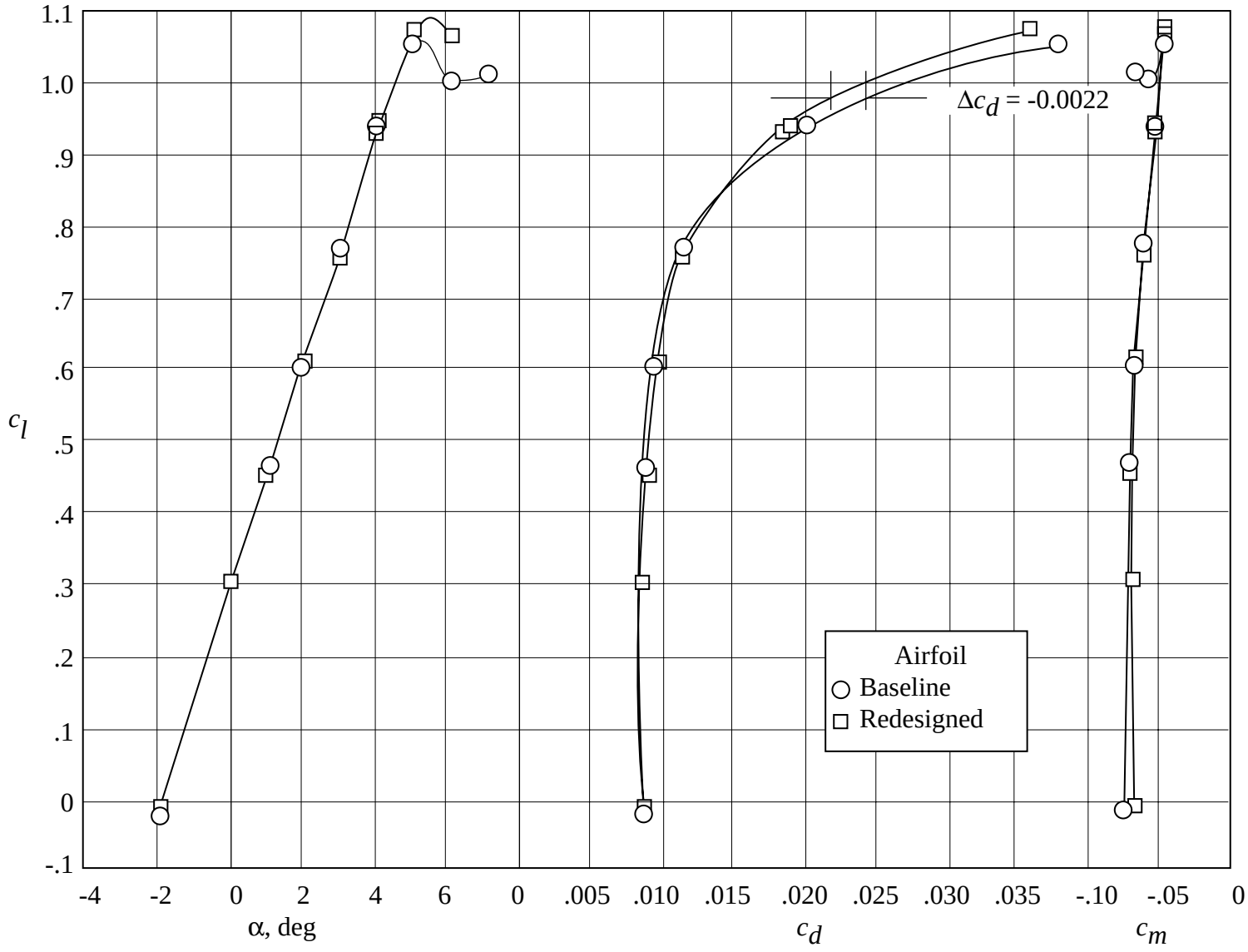
1.1
1.0
.9
.8
.7
.6
.5
.4
.3
.2
.1
0
-.1
c_l
-4
-2
0
2
4
6
α, deg
0
.005
.010
.015
.020
.025
.030
.035
c_d
Δc_d = -0.0022
-.10
-.05
0
c_m
Airfoil
Baseline
Redesigned

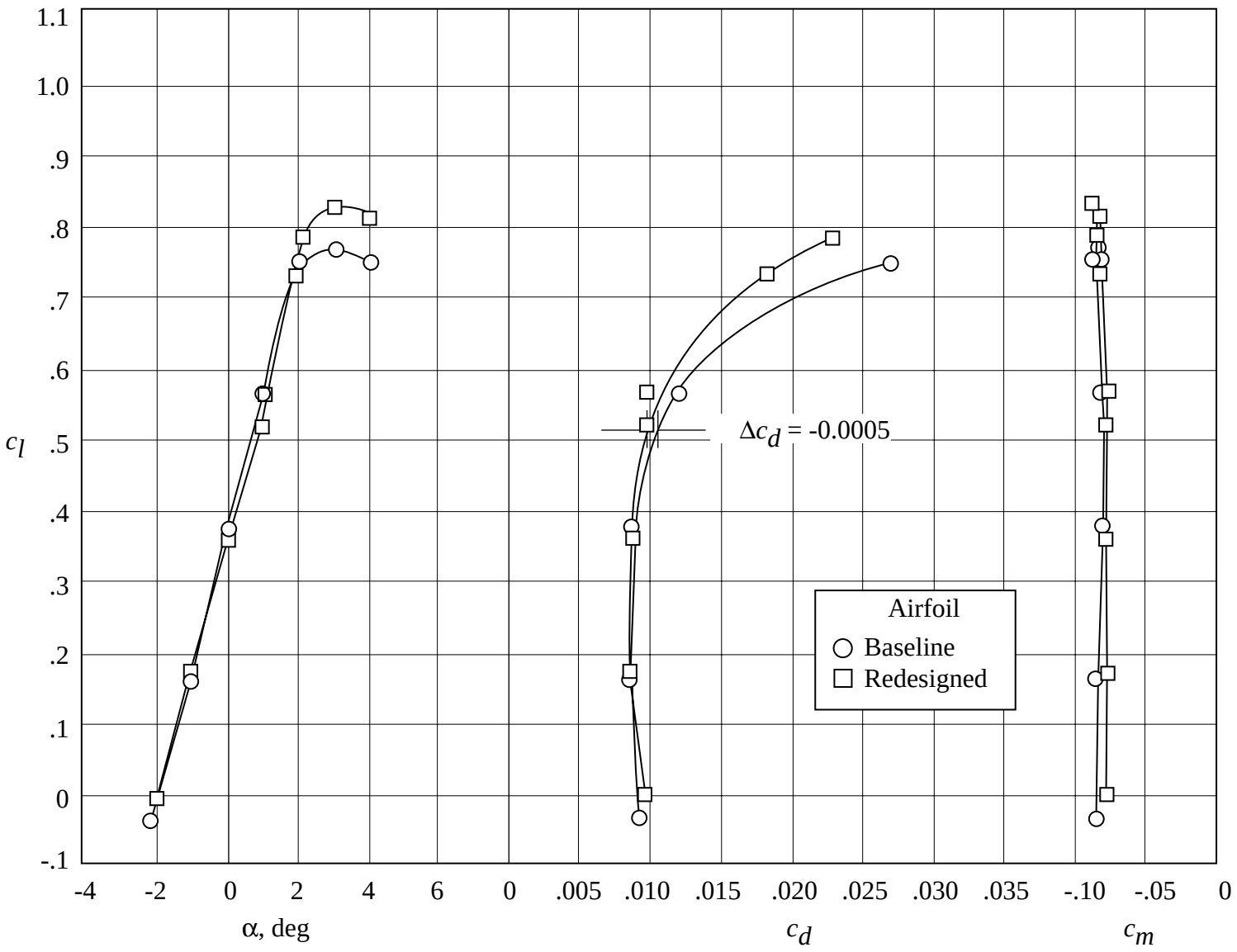
1.1
1.0
.9
.8
.7
.6
.5
.4
.3
.2
.1
0
-.1
c_l
-4
-2
0
2
4
6
α, deg
0
.005
.010
.015
.020
.025
.030
.035
c_d
Δc_d = -0.0005
-.10
-.05
0
c_m
Airfoil
Baseline
Redesigned

Figure A6. Comparison of baseline airfoil A with airfoil B (designed at long-range cruise point) and airfoil C (designed at high-speed cruise point).

(a) Climb. $M_\infty = 0.685$; $c_l = 0.850$.

(b) Cruise. $M_\infty = 0.735$; $c_l = 0.608$.

Figure 15. Comparison of analysis of baseline airfoil A with analysis of airfoil D_2 (developed after 2 cycles of airfoil shape averaging).

(a) $M_\infty = 0.654$; $R_c = 4.5 \times 10^6$.

Figure A11. Comparison of chordwise pressure distributions for baseline and redesigned airfoils. Open symbols denote upper surface; "+" within symbol denotes lower surface.

(b) $M_\infty = 0.734$; $R_c = 9.0 \times 10^6$.

Figure A11. Concluded.

(a) $M_\infty = 0.654$; $R_c = 4.5 \times 10^6$.

Figure A12. Comparison of experimental force and moment coefficients of baseline and redesigned airfoils.

(b) $M_\infty = 0.735$; $R_c = 9.0 \times 10^6$.

Figure A12. Concluded.

(a) Long-range cruise. $M_\infty = 0.654$; $c_l = 0.979$.

(b) High-speed cruise. $M_\infty = 0.735$; $c_l = 0.508$.

Figure A3. Analysis of baseline airfoil A.

(a) Long-range cruise. $M_\infty = 0.654$; $c_l = 0.977$.

(b) High-speed cruise. $M_\infty = 0.735$; $c_l = 0.508$.

Figure A4. Comparison of analysis of baseline airfoil A with analysis of airfoil B (designed at long-range cruise point).

(a) Long-range cruise. $M_\infty = 0.654$; $c_l = 0.979$.

(b) High-speed cruise. $M_\infty = 0.735$; $c_l = 0.507$.

Figure A5. Comparison of analysis of baseline airfoil A with analysis of airfoil C (designed at high-speed cruise point).

(a) Long-range cruise. $M_\infty = 0.654$; $c_l = 0.979$.

(b) High-speed cruise. $M_\infty = 0.735$; $c_l = 0.508$.

Figure A7. Comparison of analysis of redesigned airfoil I with analysis of baseline airfoil A.

Figure A8. Comparison of baseline airfoil A with redesigned airfoil I.

(a) $c_l = 0.940$; $M_\infty = 0.654$; $R_c = 4.5 \times 10^6$.

(b) $c_l = 0.565$; $M_\infty = 0.735$; $R_c = 9.0 \times 10^6$.

Figure A9. Comparison of calculated and experimental chordwise pressure distributions for baseline airfoil.

(a) $c_l = 0.940$; $M_\infty = 0.654$; $R_c = 4.5 \times 10^6$.

(b) $c_l = 0.565$; $M_\infty = 0.735$; $R_c = 9.0 \times 10^6$.

Figure A10. Comparison of calculated and experimental chordwise pressure distributions for redesigned airfoil.

Figure 2. Representation of detailed target pressure distribution with control points.

Figure 4. Multipoint design procedure using airfoil shape averaging.

Figure 6. Multipoint design procedure using target pressure averaging.

(a) Climb. $M_\infty = 0.685$; $c_l = 0.850$.

(b) Cruise. $M_\infty = 0.735$; $c_l = 0.608$.

Figure 8. Analysis of baseline airfoil A.

(a) Climb. $M_\infty = 0.685$; $c_l = 0.850$.

(b) Cruise. $M_\infty = 0.735$; $c_l = 0.608$.

Figure 9. Comparison of analysis of baseline airfoil A with analysis of airfoil B (designed at climb design point).

(a) Climb. $M_\infty = 0.685$; $c_l = 0.850$.

(b) Cruise. $M_\infty = 0.735$; $c_l = 0.608$.

Figure 10. Comparison of analysis of baseline airfoil A with analysis of airfoil C (designed at cruise design point).

Figure 11. Comparison of baseline airfoil with airfoils developed at climb and cruise design points.

(a) Climb. $M_\infty = 0.685$; $c_l = 0.850$.

(b) Cruise. $M_\infty = 0.735$; $c_l = 0.609$.

Figure 13. Comparison of analysis of baseline airfoil A with analysis of airfoil D (developed using 1 cycle of airfoil shape averaging).

Figure 14. Comparison of baseline airfoil A with airfoils developed using airfoil shape averaging.

(a) Climb. $M_\infty = 0.685$; $c_l = 0.850$.

(b) Cruise. $M_\infty = 0.735$; $c_l = 0.608$.

Figure 16. Comparison of analysis of baseline airfoil A with analysis of airfoil E (developed using target c_p averaging at climb design point).

(a) Climb. $M_\infty = 0.685$; $c_l = 0.850$.

(b) Cruise. $M_\infty = 0.735$; $c_l = 0.608$.

Figure 17. Comparison of analysis of baseline airfoil A with analysis of airfoil F (developed using target c_p averaging at cruise design point).

Figure 18. Comparison of baseline airfoil A with airfoil E (designed at climb design point) and airfoil F (designed at cruise design point).

REPORT DOCUMENTATION PAGE

Form Approved
OMB No. 0704-0188

Public reporting burden for this collection of information is estimated to average 1 hour per response, including the time for reviewing instructions, searching existing data sources, gathering and maintaining the data needed, and completing and reviewing the collection of information. Send comments regarding this burden estimate or any other aspect of this collection of information, including suggestions for reducing this burden, to Washington Headquarters Services, Directorate for Information Operations and Reports, 1215 Jefferson Davis Highway, Suite 1204, Arlington, VA 22202-4302, and to the Office of Management and Budget, Paperwork Reduction Project (0704-0188), Washington, DC 20503.

1. AGENCY USE ONLY *(Leave blank)*	2. REPORT DATE	3. REPORT TYPE AND DATES COVERED
	September 1994	Technical Paper

4. TITLE AND SUBTITLE
Application of Two Procedures for Dual-Point Design of Transonic Airfoils

5. FUNDING NUMBERS
WU 505-59-54-17

6. AUTHOR(S)
Raymond E. Mineck, Richard L. Campbell, and Dennis O. Allison

7. PERFORMING ORGANIZATION NAME(S) AND ADDRESS(ES)
NASA Langley Research Center
Hampton, VA 23681-0001

8. PERFORMING ORGANIZATION REPORT NUMBER
L-17268

9. SPONSORING/MONITORING AGENCY NAME(S) AND ADDRESS(ES)
National Aeronautics and Space Administration
Washington, DC 20546-0001

10. SPONSORING/MONITORING AGENCY REPORT NUMBER
NASA TP-3466

11. SUPPLEMENTARY NOTES

12a. DISTRIBUTION/AVAILABILITY STATEMENT
Unclassified–Unlimited

Subject Category 02

12b. DISTRIBUTION CODE

13. ABSTRACT *(Maximum 200 words)*

Two dual-point design procedures were developed to reduce the objective function of a baseline airfoil at two design points. The first procedure to develop a redesigned airfoil used a weighted average of the shapes of two intermediate airfoils redesigned at each of the two design points. The second procedure used a weighted average of two pressure distributions obtained from an intermediate airfoil redesigned at each of the two design points. Each procedure was used to design a new airfoil with reduced wave drag at the cruise condition without increasing the wave drag or pitching moment at the climb condition. Two cycles of the airfoil shape-averaging procedure successfully designed a new airfoil that reduced the objective function and satisfied the constraints. One cycle of the target (desired) pressure-averaging procedure was used to design two new airfoils that reduced the objective function and came close to satisfying the constraints.

14. SUBJECT TERMS	15. NUMBER OF PAGES
Airfoil design; Dual-point design	50
	16. PRICE CODE: A03

17. SECURITY CLASSIFICATION OF REPORT	18. SECURITY CLASSIFICATION OF THIS PAGE	19. SECURITY CLASSIFICATION OF ABSTRACT	20. LIMITATION OF ABSTRACT
Unclassified	Unclassified	Unclassified	